Quantum phase-locking and frequency down-conversion in a driven cavity-qubit system

Frederik Nathan[1], Gil Refael[2], Mark S. Rudner[1], and Ivar Martin[3]

[1]*Center for Quantum Devices, Niels Bohr Institute,*
University of Copenhagen, 2100 Copenhagen, Denmark
[2]*Institute for Quantum Information and Matter, Caltech, Pasadena, California 91125, USA*
[3] *Materials Science Division, Argonne National Laboratory, Argonne, Illinois 60439, USA*

(Dated: March 13, 2020)

We study a periodically driven qubit coupled to a quantized cavity mode. Despite its apparent simplicity, this system supports a rich variety of exotic phenomena, such as topological frequency conversion as recently discovered in [PRX **7**, 041008 (2017)]. Here we report on a qualitatively different phenomenon that occurs in this platform, namely the phase-locking of the cavity mode to a rational fraction r/q of the driving frequency Ω. The phase-locking regime is characterized by the emergence of q-tuplets of stationary (Floquet) states whose quasienergies are separated by Ω/q, up to exponentially small corrections. The Wigner functions of these states are nearly identical, and exhibit highly-regular and symmetric structure in phase space. Similarly to Floquet time crystals, these phase-locked states underlie discrete time-translation symmetry breaking in the model. We develop two complementary approaches for analyzing and predicting phase locking in the model, and use them to identify the conditions under which it occurs.

I. INTRODUCTION

In recent years, periodic driving has been explored extensively as a means for inducing exotic effects into otherwise ordinary systems[1–6]. Multiple works demonstrate that periodic driving can lead to surprising, robust phenomena without analogues in equilibrium[7–36]. These findings have inspired a wide range of experimental works, leading to the realization and observation of several of these new driving-induced phenomena, such as Floquet time crystals, and anomalous Floquet insulators[37–46]. While some of the newly discovered phenomena remain to be demonstrated, recent advances in controlling few-level quantum systems place many of these proposals within experimental reach. Promising platforms for such quantum control include cold atoms, quantum dots, superconducting qubits, electromagnetic cavities, or hybrid devices[47–49].

In this paper, we report on a new driving-induced exotic quantum effect that arises in such an experimentally accessible platform. We study a periodically-driven qubit coupled to an electromagnetic cavity, as schematically depicted in Fig. 1a. When the driving frequency Ω is tuned sufficiently close to a rational multiple q/r of the cavity's resonance frequency, the cavity-qubit system enters a regime where the system oscillates with a frequency locked exactly to $r\Omega/q$. This phase-locking persists both for weak and strong cavity-qubit coupling, and for finite windows of the driving frequency (see Fig. 1c). Hence, phase-locking is a robust effect, which does not require fine-tuning.

Classically, periodically-driven nonlinear oscillators are known to exhibit phase-locking (so-called Arnold tongues) when the driving frequency is close to a rational multiple of the oscillator's resonance frequency[32,50–53]. For quantum systems, phase locking can be understood as a breakdown of discrete time-translation sym-
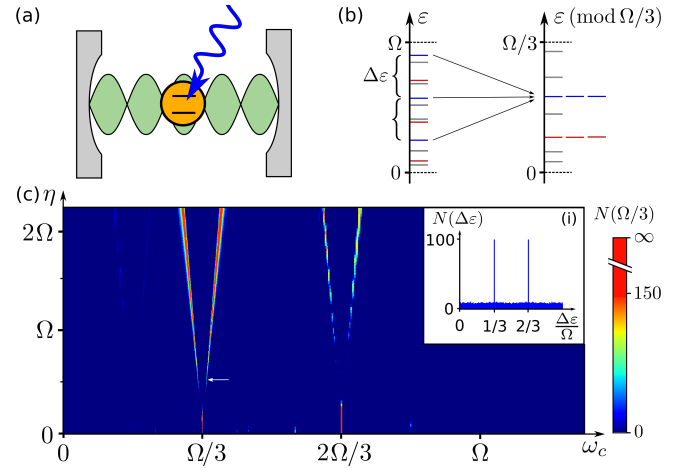

FIG. 1. a) Schematic depiction of the system we study: a 2-level system (orange) is coupled to a single cavity mode (green) along with a driving field (blue). b) illustration of quasienergy clustering (see Sec. II C for details): while the quasienergy levels of the system are effectively uniformly distributed in the interval $[0, \Omega]$, in the period-q phase-locking regime, the spacings between certain subsets of levels are exponentially close to $n\Omega/q$ for some integer n (red and blue). Here we illustrate the clustering for $q = 3$. c) Number of period-3 phase-locked Floquet eigenstates in the model, obtained from numerical exact evolution and diagonalization of the system's Floquet operator, as function of cavity frequency ω_c and qubit coupling η (see Sec. II A for model details, Sec. III for details of the simulation, and Appendix B for similar plots for other phase-locking ratios). *Inset:* histogram of quasienergy level spacings in the phase-locking regime (parameters indicated by white arrow in main panel).

metry [see also Ref. 30]. On a practical level, phase-locked quantum systems can thus be seen as examples of "Floquet time-crystals"[11,12], lending further support to

earlier suggestions[29,30,54] that time-translation symmetry breaking (in a broader sense than defined in Ref. 12) may be realized in few-body quantum systems.

Quantum phase locking is manifested through the appearance of characteristic multiplets in the system's quasienergy spectrum. Specifically, robust phase-locked oscillations of the system imply that some subsets of quasienergy levels appear in multiplets in which the levels are separated by Ω/q, up to exponentially small corrections (see sketch in Fig. 1b).

Previous works have considered phase-locking in driven quantum oscillators numerically[29], or in the weak-coupling, small-detuning limit[30]. In this paper, we develop a theory for quantum phase locking that applies beyond the limit of weak coupling and small detuning. Our analytical and numerical results demonstrate that the driven cavity-qubit system provides a versatile and experimentally-accessible platform for studying phase-locking in quantum systems.

The remainder of this paper is organized as follows: In Sec. II, we introduce the cavity-qubit model we study and analytically infer the emergence of quantum phase-locking in the model using a semiclassical approach. In Sec. III, we numerically demonstrate the existence of quantum phase-locking in the model, and explore its physical manifestations. We conclude with a discussion in Sec. IV. Technical details of derivations and additional numerics are provided in the Appendices.

II. PHASE-LOCKING IN DRIVEN QUBIT-CAVITY MODEL

In this section, we analytically infer the emergence of quantum phase locking in a driven cavity-qubit system. In Sec. II A, we introduce the model of the driven qubit-cavity system that we study. In. II B, we identify two regimes where the dynamics of the qubit may be integrated out, referred to as the adiabatic and Floquet regimes. In these two regimes, we show that, in a rotating frame, the motion of the cavity is governed by a time-independent effective Hamiltonian, H_{eff}. The effective Hamiltonian H_{eff} has a built-in symmetry that corresponds to time-translation symmetry by the period of the driving field. In Sec. II C, we show that some eigenstates of H_{eff} enable the breaking of this symmetry, giving rise to phase-locked motion in the lab frame. The analysis in this section follows the principles laid out in Ref. 30 to analyze a related phenomenon of parametric driving and period tripling of a Duffing oscillator.

In Appendix A, we present a different perspective on phase locking, based on the dynamics in the combined Fock space of the oscillator and driving field. The "photon-lattice" approach presented there is complementary to the phase-space approach presented in this section, and can be used to analyze the emergence of phase locking in the limit of small nonlinearity and detuning for a wider class of systems than the model we consider.

A. Model

Here we introduce the model for the driven qubit-cavity system that we study in this paper. The model consists of a two-level system, such as a qubit or quantum dot, coupled linearly to a cavity mode and an externally provided driving field, as schematically depicted in Fig. 1a. The cavity mode and the qubit (pseudo)spin constitute the system's degrees of freedom. The Hamiltonian of the system is given by the sum of the cavity energy and the qubit (or spin) Hamiltonian $\hat{H}_S(t)$, which includes linear coupling between cavity mode and the qubit spin:

$$\hat{H}(t) = \omega_c \hat{b}^\dagger \hat{b} + \hat{H}_S(t). \tag{1}$$

Here ω_c and $\hat{b}$ denote the frequency and bosonic annihilation operator of the cavity mode, respectively[55]. The Hamiltonian of the qubit, $\hat{H}_S(t)$, consists of three parts: a static (Zeeman) part $\hat{H}_0$, the coupling to a time-dependent driving field $\hat{V}_{\text{dr}}(t)$, and, finally, the coupling to the cavity field $\hat{H}_{SC}$:

$$\hat{H}_S(t) = \hat{H}_0 + \hat{V}_{\text{dr}}(t) + \hat{H}_{SC}. \tag{2}$$

We assume the driving field $\hat{V}_{\text{dr}}(t)$ is periodic, with period T (angular frequency $\Omega \equiv 2\pi/T$).

While we do not expect phase locking to depend on the specific details of $\hat{H}_0$, $\hat{V}_{\text{dr}}$ and $\hat{H}_{SC}$, we consider for concreteness the following form of these terms:

$$\hat{H}_0 = \eta \hat{\sigma}_x B_0, \tag{3}$$

$$\hat{V}_{\text{dr}}(t) = \eta A_d (\sin(\Omega t)\hat{\sigma}_x + \cos(\Omega t)\hat{\sigma}_z), \tag{4}$$

$$\hat{H}_{SC} = \eta (\hat{b}\hat{\sigma}^+ + \hat{b}^\dagger \hat{\sigma}^-). \tag{5}$$

Here η has units of energy, and gives the scale of the coupling between the qubit and the fields (both static and dynamic) [see Eq. (6) below], while the Pauli matrices $\hat{\sigma}_x, \hat{\sigma}_y, \hat{\sigma}_z$ act on the qubit's spin, with $\hat{\sigma}^\pm \equiv \frac{1}{2}(\hat{\sigma}_x \pm i\hat{\sigma}_y)$. Finally, B_0 and A_d are dimensionless numbers denoting the effective Zeeman field strength and driving amplitude, respectively. This model was previously studied in the context of topological frequency conversion in Refs. 13 and 14.

In the following discussion, it is convenient to use the dimensionless position and momentum basis for the cavity[56], $\hat{x} \equiv \frac{1}{2}(\hat{b} + \hat{b}^\dagger)$ and $\hat{p} \equiv \frac{1}{2i}(\hat{b} - \hat{b}^\dagger)$. In terms of these, the Hamiltonian of the system is given by

$$\hat{H}(t) = \frac{\omega_c}{2}(\hat{x}^2 + \hat{p}^2) + \eta \mathbf{b}(\hat{x}, \hat{p}, t) \cdot \hat{\mathbf{S}}, \tag{6}$$

where $\hat{\mathbf{S}} = (\hat{\sigma}_x, \hat{\sigma}_y, \hat{\sigma}_z)$ denotes the qubit spin, while

$$\mathbf{b}(x, p, t) = (B_0 - A_d \sin\Omega t - x, p, A_d \cos\Omega t) \tag{7}$$

denotes the effective magnetic field acting on the qubit's spin. The latter quantity will play an important role throughout this work.

The class of models presented here can be realized in various ways. Most appealing perhaps are realizations using superconducting qubits[49,57,58]. Alternatives are nitrogen-vacancy (NV) centers[59,60] as well as atoms in optical cavities (see, e.g., Refs. 61 and 62). While in this paper we consider coupling the qubit spin to a single cavity mode, we expect that the discussion below generalizes to cavities with multiple modes[14].

B. Effective cavity Hamiltonian

The qubit-cavity model above supports phase locking when the drive frequency Ω is close to a rational multiple q/r of the cavity resonance frequency ω_c, where q and r are integers. In this subsection, we analyze the system's dynamics of in this regime. We go to a frame where the phase space of the cavity mode rotates with frequency $r\Omega/q$. In this rotating frame, we identify two regimes, referred to as the adiabatic and Floquet regimes, where the dynamics of the cavity mode is well-described by a time-independent effective Hamiltonian, H_{eff}. In Sec. II C, we show that nontrivial stationary orbits of this effective Hamiltonian give rise to phase-locked motion in the lab frame.

The dynamics of the qubit-cavity system are conveniently analyzed in terms of the system's Floquet operator $\hat{U}(T)$, where $\hat{U}(t) \equiv T e^{-i \int_0^t dt' \hat{H}(t')}$ defines the system's time-evolution operator and $\mathcal{T}$ denotes the time-ordering operation. The Floquet operator evolves any initial state $|\psi(0)\rangle$ through an integer number of driving periods k as $|\psi(kT)\rangle = [\hat{U}(T)]^k |\psi(0)\rangle$. In particular, after each driving period, the eigenstates of the Floquet operator, $\{|\psi_n\rangle\}$, known as the Floquet eigenstates, are mapped to themselves up to unitary phases: $\hat{U}(T)|\psi_n\rangle = e^{-i\varepsilon_n T}|\psi_n\rangle$. Here the real-valued quantity ε_n, known as quasienergy, plays a role analogous to energy for the evolution of the system, but is only defined modulo Ω. Within a driving period the time-evolution of a Floquet eigenstate $|\psi_n\rangle$ is given by $\hat{U}(t)|\psi_n\rangle = e^{-i\varepsilon_n t}|\phi_n(t)\rangle$, where $|\phi_n(t)\rangle = |\phi_n(t+T)\rangle$ is time-periodic and satisfies $|\phi_n(0)\rangle = |\psi_n\rangle$. The states $\{|\phi_n(t)\rangle\}$ are known as the Floquet, or micromotion, states.

The Floquet eigenstates and quasienergies define a time-independent effective (Floquet) Hamiltonian $\hat{H}_{\text{eff}} \equiv \sum_n \varepsilon_n |\psi_n\rangle\langle\psi_n|$ that generates the stroboscopic dynamics of the system[63] (i.e., the evolution of the system over integer multiples of the driving period T). Specifically, using $\hat{U}(T) = e^{-i\hat{H}_{\text{eff}}T}$, we have $|\psi(nT)\rangle = e^{-i\hat{H}_{\text{eff}}nT}|\psi(0)\rangle$. This subsection aims to obtain an effective Hamiltonian for the system in or near the regime of phase locking.

To obtain a time-independent effective Hamiltonian for the system, we transform to a rotating frame where the oscillator phase space rotates with angular velocity $\tilde{\Omega} \equiv r\Omega/q$, using the the Hamiltonian $\hat{H}_R = \tilde{\Omega}\hat{b}^\dagger\hat{b}$. In this rotating frame, the system evolves with the Hamiltonian $\tilde{H}(t) = \hat{U}_0^\dagger(t)[\hat{H}(t) - \hat{H}_R]\hat{U}_0(t)$, where $\hat{U}_0(t) \equiv e^{-i\hat{H}_R t}$;

the Schrödinger equation in the lab frame is solved by $|\psi(t)\rangle = \hat{U}_0(t)|\tilde{\psi}(t)\rangle$, where $\partial_t|\tilde{\psi}(t)\rangle = -i\tilde{H}(t)|\tilde{\psi}(t)\rangle$. Noting that $\hat{U}_0(t)$ only acts nontrivially on $\hat{H}_{SC}$, we find

$$\tilde{H}(t) = \frac{\delta\omega}{2}(\hat{x}^2 + \hat{p}^2) + \eta\mathbf{h}(\hat{x}, \hat{p}, t) \cdot \hat{\mathbf{S}}. \tag{8}$$

Here $\delta\omega \equiv \omega_c - \tilde{\Omega}$ denotes the detuning of the cavity frequency from $\tilde{\Omega}$, while $\mathbf{h}$ is obtained from $\mathbf{b}$ in Eqs. (6) and (7) after rotating the oscillator phase space by $\tilde{\Omega}t$: $\mathbf{h}(x, p, t) = \mathbf{b}(x\cos\tilde{\Omega}t + p\sin\tilde{\Omega}t, p\cos\tilde{\Omega}t - x\sin\tilde{\Omega}t, t)$.

Due to the explicit time-dependence of $\mathbf{h}(x, p, t)$, the rotating frame Hamiltonian $\tilde{H}(t)$ describes a periodically driven system with extended period qT (recall that $\tilde{\Omega} = r\Omega/q$). Letting $\hat{V}(t) \equiv \mathcal{T}e^{-i\int_0^t dt' \tilde{H}(t')}$ denote the rotating frame time-evolution operator generated by $\tilde{H}(t)$, the relations above Eq. (8) imply that $\hat{U}(t) = \hat{U}_0(t)\hat{V}(t)$. Since the uniform spectral spacing $r\Omega/q$ of $\hat{H}_R$ implies $\hat{U}_0(qT) = 1$, we thus have $V(qT) = \hat{U}^q(T)$. As a result, we conclude that the Floquet eigenstates of the T-periodic lab-frame Hamiltonian $\hat{H}(t)$ are identical to the Floquet eigenstates of the qT-periodic rotating frame Hamiltonian $\tilde{H}(t)$. The corresponding quasienergies of the two Hamiltonians are identical modulo $\tilde{\Omega}$.

The crucial advantage of the rotating frame transformation is that the evolution of the cavity now takes place on the timescales $\delta\omega^{-1}, \eta^{-1}$, which can be much longer than the driving period qT in (8). This separation of time scales allows us to eventually integrate out the spin and the driving field.

To analyze the system's dynamics in the rotating frame, we consider the equations of motion generated by $\tilde{H}(t)$ for the Heisenberg picture operators $\hat{x}(t)$, $\hat{p}(t)$, and $\hat{\mathbf{S}}(t)$:

$$\partial_t\hat{x}(t) = \delta\omega\hat{p}(t) + \eta\partial_p\mathbf{h}(t) \cdot \hat{\mathbf{S}}, \tag{9}$$

$$\partial_t\hat{p}(t) = -\delta\omega\hat{x}(t) - \eta\partial_x\mathbf{h}(t) \cdot \hat{\mathbf{S}} \tag{10}$$

$$\partial_t\hat{\mathbf{S}}(t) = \eta\mathbf{h}[\hat{x}(t), \hat{p}(t), t] \times \hat{\mathbf{S}}, \tag{11}$$

where, for $s = x, p$, $\partial_s\mathbf{h}(t) \equiv \partial_s\mathbf{h}(x, p, t)$. Note that $\partial_s\mathbf{h}(t)$ is a vector with unit norm, independent of x and p: for example, $\partial_x\mathbf{h}(x, p, t) = (-\cos\tilde{\Omega}t, \sin\tilde{\Omega}t, 0)$, $\partial_p\mathbf{h}(x, p, t) = (\sin\tilde{\Omega}t, \cos\tilde{\Omega}t, 0)$ [see definition of $\mathbf{h}$ below Eq. (8) and in Eq. (7)].

As the next step toward obtaining a time-independent effective Hamiltonian for the system, we consider the semiclassical dynamics of the system. In Eq. (11), we approximate $\mathbf{h}(\hat{x}(t), \hat{p}(t), t) \approx \mathbf{h}(x(t), p(t), t)$, where $x(t) \equiv \langle\hat{x}(t)\rangle$, and $p(t) \equiv \langle\hat{p}(t)\rangle$. We expect this semiclassical approximation to be justified when the characteristic scales in phase space associated with $\mathbf{h}(x, p, t)$ is large compared to the scale of quantum fluctuations $\Delta x, \Delta p \sim 1$. After this approximation, Eq. (11) reduces to a Bloch-equation with a time-dependent field $\mathbf{h}(x(t), p(t), t)$. By taking the expectation values on both sides of Eqs. (9)-(11), and recalling that $\partial_s\mathbf{h}(t)$ is a three-component vector of scalars, we then obtain 3 coupled equations of motion for the
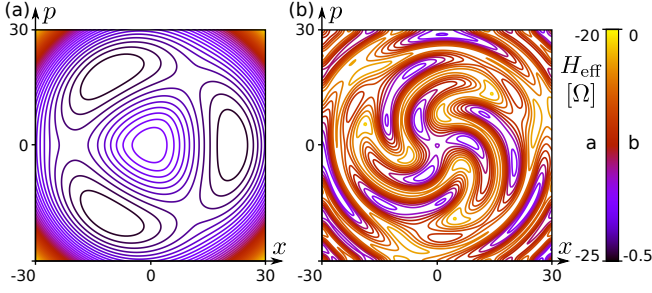
FIG. 2. Contour plots of the effective cavity Hamiltonian for the two phase-locking regimes discussed in Sec. II B. (a) Constant (quasi)energy contours of $H_{\text{eff}}(x,p)$ in the adiabatic regime, for anti-aligned spin [Eq. (17) with sign $-$]. (b) Constant (quasi)energy contours of $H_{\text{eff}}(x,p)$ in the Floquet regime, for anti-aligned spin [Eq. (19)] with sign $-$]. See Secs. II B and II B 2 for parameters in the adiabatic and Floquet regimes, respectively.

(semi-)classical variables $x(t), p(t)$, and $\mathbf{S}(t) \equiv \langle \mathbf{S}(t) \rangle$: namely Eqs. (9)-(11) with the operators $\hat{x}(t), \hat{p}(t)$, and $\hat{\mathbf{S}}(t)$ substituted by their expectation values $x(t), p(t)$, and $\mathbf{S}(t)$.

Having established the semiclassical equations of motion for the qubit-cavity system, we now identify two regimes where the qubit spin $\mathbf{S}(t)$ can effectively be integrated out, thus resulting in self-contained equations of motion for the cavity mode alone. Subsequently using a separation of timescales between the cavity's dynamics and the driving frequency in these equations of motion, we obtain *time-independent* effective Hamiltonians that describe the cavity's motion in these regimes. We use these effective Hamiltonians to infer the existence of phase locking in Sec. II C.

1. Adiabatic regime

The first situation where the qubit spin can be integrated out is the case where the field $\mathbf{h}(x(t), p(t), t)$ rotates adiabatically on the time scale of Larmor precession of the spin, $\mathbf{S}$. Specifically when the spin's instantaneous precession frequency $f_{\text{spin}} \equiv \eta |\mathbf{h}(x,p,t)|$ is much larger than $\frac{d\mathbf{n}}{dt}$ where $\mathbf{n} = \mathbf{h}/|\mathbf{h}|$, the adiabatic theorem states that $\mathbf{S}(t) \cdot \mathbf{h}(x(t), p(t), t)$ remains nearly constant for exponentially long times. In particular, if $\mathbf{S}(t = 0)$ is initially aligned or antialigned with $\mathbf{h}(x(0), p(0), 0)$, its evolution at later times $\mathbf{S}(t)$ will satisfy

$$\mathbf{S}(t) \approx \pm \frac{\mathbf{h}(x(t), p(t), t)}{|\mathbf{h}(x(t), p(t), t)|}, \tag{12}$$

where the sign depends on the initial alignment. Using Eq. (12) in Eqs. (9) and (10), we obtain the following self-contained equations of motion for the cavity:

$$\dot{x}(t) = v_x(x,p,t), \quad \dot{p}(t) = -v_p(x,p,t), \tag{13}$$

where

$$v_x(x,p,t) \equiv \delta\omega p \pm \eta \partial_p |\mathbf{h}(x,p,t)|, \tag{14}$$
$$v_p(x,p,t) \equiv \delta\omega x \pm \eta \partial_x |\mathbf{h}(x,p,t)|. \tag{15}$$

As above, the signs depend on the initial alignment of the spin with the field. In Appendix C we show that these equations of motion are generally valid in regions of phase space where $|\mathbf{h}(x,p,t)| \gg 1$, $\tilde{\Omega}/\eta$ for all t[64].

Next, we identify the conditions under which the state of the cavity mode (in the rotating frame!) remains effectively stationary within a driving period. Specifically, we seek the conditions under which $\Delta x(t), \Delta p(t) \ll A_{\text{cav}}$ for $t \le qT$, where $\Delta x(t) = x(t) - x(0)$ and $\Delta p(t) = p(t) - p(0)$, while $A_{\text{cav}} = \sqrt{x^2 + p^2}$ denotes the amplitude of the cavity field. When x and p change slowly within a driving period, we may assume the first two arguments of v_x and v_p in Eqs. (14)-(15) stationary within the driving period qT, and thus approximate them by their values at $t = 0$. From Eq. (13), we then have $\partial_t \Delta x(t) \lesssim |v_x(x(0), p(0), t)|$. Using $\partial_p |\mathbf{h}| = 1$[65] in Eq. (14), we find $|v_x(x,p,t)| \le \delta\omega A_{\text{cav}} + \eta$. Thus $|\Delta x(t)| \lesssim (\delta\omega A_{\text{cav}}(0) + \eta)qT$. The same bound holds for $\Delta p(t)$. We conclude that the cavity is effectively stationary within a driving period when $(\delta\omega A_{\text{cav}} + \eta)qT \ll A_{\text{cav}}$.

When the condition above is realized, the cavity evolution takes place on a much longer timescale than qT. Hence, for $s = x, p$, only the quasistatic components $\bar{v}_s(x,p) \equiv \frac{1}{qT} \int_0^{qT} dt\, v_s(x,p,t)$ contribute to $\dot{s}$ in Eq. (13)

$$\dot{x} \approx \bar{v}_p(x,p), \quad \dot{p} \approx -\bar{v}_x(x,p). \tag{16}$$

By writing $\bar{v}_s(x,p) = \partial_s H_{\text{eff}}(x,p)$, we identify

$$H_{\text{eff}}(x,p) = \frac{\delta\omega}{2}(x^2 + p^2) \pm \frac{\eta}{qT} \int_0^{qT} dt\, |\mathbf{h}(x,p,t)|. \tag{17}$$

We expect the time-independent effective Hamiltonian $H_{\text{eff}}(x,p)$ in Eq. (17) to describe the cavity's dynamics when the condition $(\delta\omega A_{\text{cav}} + \eta)qT \ll A_{\text{cav}}$ described above is satisfied.

Note that the last term in Eq. (17) modifies the phase space energy landscape for the oscillator. For large amplitudes, this modification effectively shifts the angular velocity of the oscillator state in phase space by an amount $\pm\eta\kappa(x,p)$, where $\kappa(x,p)$ is given by $1/A_{\text{cav}}$ times the radial component of the gradient of the second term in Eq. (17) [i.e., the derivative along the direction connecting the origin to phase space point (x,p)]. We expect the cavity to be stationary within a driving period in regions of phase-space where the frequency shift above approximately compensates the contribution to $\dot{x}$ and $\dot{p}$ from the finite detuning $\delta\omega$. We hence expect the effective Hamiltonian in Eq. (17) to capture the dynamics of the cavity mode (in the rotating frame) as long as the conditions above are satisfied by the *renormalized* detuning $\delta\omega' = \delta\omega \pm \eta\kappa(x,p)$ (rather than the "bare" detuning $\delta\omega$).

With the renormalization of the cavity frequency included, the conditions for the adiabatic regime are

1, $\Omega/\eta \ll A_{\text{cav}}$, and $\delta\omega', \eta/A_{\text{cav}} \ll \Omega$. where we used $|\mathbf{h}| \sim A_{\text{cav}}$, and $\tilde{\Omega} \sim \Omega$. Here the first two conditions ensure that the effective field acting on the spin $\mathbf{h}(x,p,t)$ changes adiabaticity, while two latter conditions ensure that the cavity can be assumed stationary within the driving period qT, thus allowing us to integrate out the time-dependence of $\mathbf{h}$. Noting that $1 \leq \max(a, a^{-1})$ for any positive number a, we summarize the conditions as follows:

$$\eta/\Omega, \ \Omega/\eta \ll A_{\text{cav}}, \quad \delta\omega' \ll \Omega. \tag{18}$$

Using that $\delta\omega'$ is given by the $1/A_{\text{cav}}$ times the radial gradient of H_{eff}, the second condition above is in particular satisfied in regions of phase space close to the extrema and saddle points of H_{eff}

For illustration, in Fig. 2a we plot the constant (quasi)energy contours of H_{eff} with $q = 3$ and $r = 1$, for antialigned spin (with sign $-$), and parameters $A_d = 15$, $B_0 = 7$, $\omega_c = 0.34\Omega$ and $\eta = 0.56\Omega$. Since $\eta/\Omega \approx 0.56$, $H_{\text{eff}}(x,p)$ should provide an accurate description of the system's dynamics when $\delta\omega' \ll \Omega$ and $A_{\text{cav}} \gg \Omega/\eta = 1.8$. In particular, we expect H_{eff} to describe the system accurately near the three minima located at radius $A_{\text{cav}} \approx 24$, where its gradient (and hence $\delta\omega'$) vanishes.

2. Floquet regime

The second regime where the dynamics of the cavity mode are well-described by a static effective Hamiltonian is referred to as the Floquet regime, and has a more subtle origin than the adiabatic regime above: whereas the adiabatic regime arises when the instantaneous Hamiltonian of the spin changes adiabatically, the Floquet regime occurs when the effective *Floquet* Hamiltonian of the spin (with x and p fixed) changes adiabatically. The derivation of the effective Floquet Hamiltonian proceeds along similar lines as for the adiabatic regime in Sec. II B. Here we give a heuristic derivation of the results, while a more rigorous derivation is given in Appendix C 2.

To obtain the effective Hamiltonian, we consider the dynamics resulting from Eq. (11) for fixed x and p. In this case, the time-periodicity of $\mathbf{h}(x,p,t)$ implies that all solutions to Eq. (11) satisfy $\mathbf{S}([n+1]\tilde{T}) = R_0(x,p)\mathbf{S}(n\tilde{T})$, for a fixed three-dimensional (3d) rotation matrix $R_0(x,p)$. The 3d rotation matrix generates a rotation about some axis $\mathbf{a}(x,p)$ by an angle $\theta(x,p) \equiv \varepsilon(x,p)qT$. As a result, there exists a time-periodic solution to the Bloch equation in Eq. (11) (up to a constant scale factor), $\mathbf{S}(t) = \mathbf{n}_0(x,p,t)$, in which $\mathbf{n}_0(x,p,0) = \mathbf{a}(x,p)$ is parallel to the net rotation axis, and $\mathbf{n}_0(x,p,t)$ evolves according to Eq. (11). Thus, for fixed x and p, we identify $H_{\text{eff}}^{\text{spin}}(x,p) = \varepsilon(x,p)\mathbf{a}(x,p) \cdot \mathbf{S}$ as the effective Hamiltonian of the spin (see Appendix C 2 for further details). When x and p are not fixed, but the state of the cavity field evolves slowly in comparison with the "quasienergy gap" of $H_{\text{eff}}^{\text{spin}}$, $\delta\varepsilon = \min_z(|\varepsilon + z\Omega|)$, the

stroboscopic motion of the spin closely follows stroboscopic motion resulting from the adiabatically changing Hamiltonian $H_{\text{eff}}^{\text{spin}}(x(t), p(t))$[66]. As a result, if initially aligned or anti-aligned with $\mathbf{a}(x(0), p(0))$, the spin's evolution at later (stroboscopic) times will satisfy $\mathbf{S}(n\tilde{T}) \approx \pm\mathbf{a}(x(n\tilde{T}), p(n\tilde{T}))$, and at intermediate times will be given by $\mathbf{S}(t) \approx \mathbf{n}_0(x(t), p(t), t)$ following Eq. (11). Substituting this into Eqs. (9)-(10) and time-averaging the resulting equations of motion (since the cavity mode will also be stationary on the time-scale qT), we show in Appendix C 2 that $\dot{x} \approx \partial_p H_{\text{eff}}(x,p)$ and $\dot{p} \approx -\partial_x H_{\text{eff}}(x,p)$ where

$$H_{\text{eff}}(x,p) = \frac{\delta\omega}{2}\left(x^2 + p^2\right) \pm \varepsilon(x,p). \tag{19}$$

Here $\varepsilon(x,p)$ denotes the stroboscopic rotation angle above, and is given by

$$\varepsilon(x,p) = \frac{\eta}{\tilde{T}} \int_0^{\tilde{T}} dt\, \mathbf{n}_0(x,p,t) \cdot \mathbf{h}(x,p,t) + \frac{1}{\tilde{T}}\gamma(x,p), \tag{20}$$

where $\gamma(x,p)$ is the Berry phase associated with the closed trajectory of $\mathbf{n}_0(x,p,t)$ for a fixed x and p [i.e., half the area on the unit sphere enclosed by $\mathbf{n}_0(x,p,t)$ for $0 \leq t < qT$]. Hence, the stroboscopic evolution of the cavity mode (in the rotating frame) is described by the time-independent effective Hamiltonian $H_{\text{eff}}(x,p)$ above.

We identify the conditions for the Floquet regime in Appendix C 2, and find that the results above are valid when

$$\eta, \ \sqrt{\eta\delta\omega A_{\text{cav}}} \ll \delta\varepsilon, \quad \eta/A_{\text{cav}}, \ \delta\omega \ll \Omega. \tag{21}$$

The quasienergy gap $\delta\varepsilon$ for the spin depends nontrivially on the parameters of the Hamiltonian and the location in phase space, but can be easily computed numerically through exact diagonalization of the 3×3 rotation matrix $R_0(x,p)$. The characteristic scale for this quantity is half the Floquet Brillouin zone width $\tilde{\Omega}/2 = \Omega/2q$.

We note that nontrivial winding of the term $\gamma(x,p)$ in Eq. (20) as a function of x and p can give rise to topological pumping effects, as reported in Ref. 13 and 14. We will not pursue this possibility further here, but leave such an investigation for future work.

In Fig. 2b, we plot the contours of $H_{\text{eff}}(x,p)$ for antialigned spin (with sign $-$) for the parameters $A_d = 15, B_0 = 7, \omega_c = \Omega/3$ and $\eta = 0.048\Omega$. Since $\delta\omega = 0$, the conditions above imply that this effective Hamiltonian accurately describes the dynamics whenever $\min_z |H_{\text{eff}}(x,p) - z\Omega| \gg \eta$ and $A_{\text{cav}} \gg \eta/\Omega$. Using $\eta = 0.048\Omega$, we see that this condition is satisfied when $|H_{\text{eff}}(x,p)| \gg 0.048\Omega$ and $A_{\text{cav}} \gg 0.048$.

C. Phase locking

Here we infer the emergence of phase locking from the existence of the time-independent effective Hamiltonian

$H_{\text{eff}}(x,p)$ in Sec. II B, following a line of arguments similar to those laid out in Ref. 30. For concreteness we focus on the case where Ω is close to $3\omega_c$, i.e., $q/r = 3/1$, while we note that phase locking can occur at any rational multiple q/r (see Appendix B).

In Sec. II B, we identified two regimes where the cavity mode's evolution is governed by a time-independent effective Hamiltonian $H_{\text{eff}}(x,p)$ in a frame where phase space rotates with angular frequency $\Omega/q = \Omega/3$ [Eqs. (17) and (19)]. In this rotating frame, the value of $H_{\text{eff}}(x,p)$ must be conserved by the dynamics; the cavity evolution must therefore follow the one-dimensional constant (quasi)energy contours of $H_{\text{eff}}(x,p)$ in phase space. Importantly, the effective Floquet Hamiltonian $H_{\text{eff}}(x,p)$ is by construction symmetric under C_3 rotations in phase space. To see this, note that $\mathbf{h}(x',p',t) = \mathbf{h}(x,p,t+T)$, where (x',p') is related to x and p through phase-space rotation by $2\pi/3$. The same symmetry applies to $\mathbf{n}_0(x,p,t)$ in Eq. (20), since $\mathbf{n}_0(x,p,t)$ is uniquely determined from $\mathbf{h}$. Due to the fact that the integrals in Eq. (20) are invariant under time-translations, $H_{\text{eff}}(x,p)$ thus exhibits C_3 rotation symmetry in phase space. The C_3 rotation symmetry of $H_{\text{eff}}(x,p)$ in the rotating frame corresponds to the time-translation symmetry by T in the lab frame. This symmetry is clearly evident in Figs. 2ab, where we show the constant (quasi)energy contours of H_{eff} for two parameter sets with $\Omega \approx 3\omega_c$.

Figs. 2ab show that the effective Hamiltonian $H_{\text{eff}}(x,p)$ can have local extrema at nonzero values of x and p. Due to the C_3 rotation symmetry of H_{eff}, these extrema must come in groups of 3. The qubit-cavity system enters the phase-locked regime when its wavefunction is initialized in a "potential well" of H_{eff} (note that for non-dissipative cases, these "potential wells" also include regions near local maxima). In this case, since the motion of the system in the rotating frame must conserve H_{eff}, its wavefunction $|\tilde{\psi}(t)\rangle$ remains confined in the potential well for an exponentially long time. The duration of the confinement τ_c is determined by the quantum tunneling between the potential wells of $H_{\text{eff}}(x,p)$. This rate is exponentially suppressed in d/ξ, where d denotes the separation between the potential wells in phase space, and $\xi \sim 1$ denotes the scale of quantum fluctuations.

To see how the confinement of $|\tilde{\psi}(t)\rangle$ in a potential well of H_{eff} implies phase-locking, consider the dynamics of the wavefunction in the lab frame $|\psi(t)\rangle = \hat{U}_0(t)|\tilde{\psi}(t)\rangle$ [see above Eq. (8)]. Recalling that $\hat{U}_0(T)$ generates a phase-space rotation by $2\pi/3$, after k periods the time-evolved wavepacket $|\psi(kT)\rangle = [U_0(T)]^k|\tilde{\psi}(kT)\rangle$ only has support in potential well $k \pmod 3$. As a result, the frequency spectrum of any observable will have a sharp peak at frequency $\Omega/3$, and the system is in the phase-locking regime.

The existence of the phase-locking regime above has highly nontrivial implications of the Floquet states and quasienergy spectrum of the system. To see this, consider the Floquet eigenstate decomposition of the initial state in a single well $|\psi(0)\rangle = \sum_n c_n|\psi_n\rangle$, where

$\{|\psi_n\rangle\}$ denote the Floquet eigenstates of the system in the lab frame. When restricting ourselves to regions of phase space where $A < A_0$, the Hilbert space is spanned by $D \sim 2A_0^2$ states, and at least one of the coefficients c_{n_0} has magnitude larger than $1/\sqrt{D}$. Using $|\psi(kT)\rangle = \sum_n c_n e^{-i\varepsilon_n kT}|\psi_n\rangle$, we consider the state

$$|\phi\rangle \equiv \frac{1}{N}\sum_{k=1}^{N} e^{ik\varepsilon_{n_0}T}|\psi(kT)\rangle. \qquad (22)$$

for some $N \ll \tau_c/T$, where τ_c denotes the exponentially large tunneling time between the potential wells of H_{eff}. One can verify that, for $N \gg D$, $|\phi\rangle = c_{n_0}|\psi_{n_0}\rangle + |\delta\phi\rangle$, where $|\delta\phi\rangle$ denotes the component of $|\phi\rangle$ orthogonal to $|\phi_{n_0}\rangle$, and has norm of order $1/N$. Letting $\lambda \equiv \langle\phi|\phi\rangle$ denote the norm of $|\phi\rangle$, we conclude that $\lambda = |c_{n_0}| + \mathcal{O}(c_{n_0}^{-1}N^{-2})$. Using $|c_n| \geq 1/\sqrt{D}$, we conclude that the normalized state $|\phi\rangle/\lambda$ is identical to $|\psi_{n_0}\rangle$, up to a correction whose norm is of order $\lesssim \sqrt{D}/N^2$. When the wells are well-separated, N can be exponentially large (much larger than $D \sim A_0^2$). As a result, the normalized state $|\phi\rangle/\lambda$ will in this case be identical to the Floquet eigenstate $|\psi_{n_0}\rangle$, up to a negligible correction.

To demonstrate the existence of phase-locked Floquet states, we write $|\phi\rangle = |\chi_1\rangle + |\chi_2\rangle + |\chi_3\rangle$, where $|\chi_m\rangle$ consists of the terms in Eq. (22) with $k = m \pmod 3$. Since for $k \leq N$, the state $|\psi(kT)\rangle$ only has support in well $k \pmod 3$, $|\chi_m\rangle$ also only has support in well m. As a result, the states $|\chi_m\rangle$ for $m = 1,2,3$ are orthogonal, up to exponentially small corrections (due to the exponentially decaying tails of the wavefunctions outside their respective potential wells). Now consider the state $|\phi'\rangle = |\chi_1\rangle + e^{-2\pi i/3}|\chi_2\rangle + e^{-4\pi i/3}|\chi_3\rangle$. Due to the near-orthogonality of the states $\{|\chi_m\rangle\}$, one can verify that $\langle\phi'|\phi'\rangle \approx \langle\phi|\phi\rangle = \lambda^2$. Moreover, by direct computation, one can verify that $U(T)|\phi'\rangle = e^{-\varepsilon_n + \Omega/3}|\phi'\rangle + \mathcal{O}(1/N)$. We conclude that $|\phi'\rangle/\lambda$ is a normalized Floquet eigenstate of U, up to a negligible correction of order $\sqrt{D}/(N)$.

We conclude that, for each Floquet eigenstate $|\psi_{n_0}\rangle$ with support in a potential well of H_{eff} (given properly aligned spin), there exists another Floquet eigenstate with support in the same potential well whose quasienergy differs from that of $|\psi_{n_0}\rangle$ by $\Omega/3$, up to an exponentially suppressed correctin of order $1/\tau_c \sim \mathcal{O}(e^{-d/\xi})$. By iteration, we conclude that $|\psi_{n_0}\rangle$ must form a part of a triplet of Floquet eigenstates $|\Psi_1\rangle, |\Psi_2\rangle, |\Psi_3\rangle$, whose quasienergies differ by *exactly* $\Omega/3$, up to an exponentially suppressed correction on the order of $1/\tau_c \sim e^{-d/\xi}$. Following the arguments above, this triplet of states can be written in the form

$$|\Psi_\nu\rangle = \sum_{m=1}^{3} e^{-2\pi i\nu m/3}|\chi_m\rangle, \qquad (23)$$

where $|\chi_m\rangle$ has support only in well m. The phase-locking mechanism above occurs when either of the effective Hamiltonians $H_{\text{eff}}(x,p)$ from Eqs. (17) or (19)
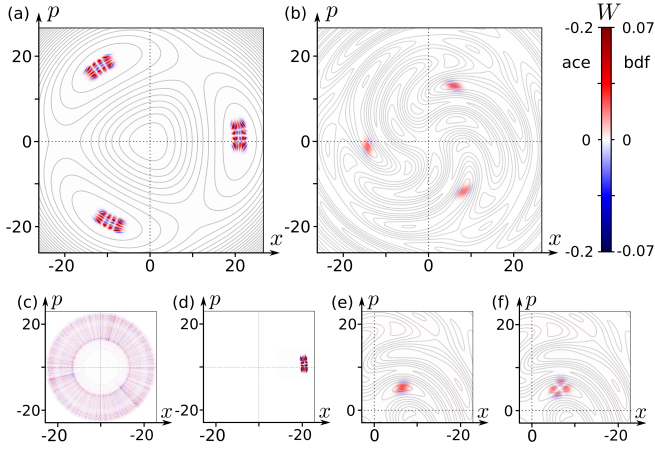
FIG. 3. Wigner functions of phase-locked Floquet eigenstates, with contours of the corresponding effective Hamitonians shown as grey lines (see Figs. 2). (a) Wigner function for a period-3 phase-locked Floquet eigenstate in the adiabatic regime, with the same parameters as used in Fig. 2a. (b) Wigner function for a period-3 phase locking Floquet eigenstate in the Floquet regime, with the same parameters as used in Fig. 2b. (c) Wigner function of a typical non-phase-locking Floquet eigenstate, for the same parameters as used in panel (b). (d) Wigner function for an equal-weight linear combination of the 3 phase-locked Floquet eigenstates, one of them being the state in (b). (e,f) Wigner functions of additional phase-locking Floquet eigenstates located in a distinct potential well of the effective Hamilton, for the same parameters as used in panel (a). Note that only the first quadrant of phase space is shown.

has well-separated local extrema in regions of phase space where the respective conditions for validity [Eqs. (18) or (21)] are satisfied.

III. NUMERICAL RESULTS

In this section, we support the conclusions from the analytical discussion in Sec. II with numerical results.

We computed the complete Floquet operator of the qubit-cavity model (see Sec. II A) using direct time-evolution, and obtained the quasienergy spectrum and Floquet eigenstates through exact diagonalization. We initially chose the parameters $B_0 = 7$, $A_d = 15$, $\eta = 0.561\Omega$, and $\omega_c = 0.343\Omega$, the values of the latter two parameters indicated by the white arrow in Fig. 1c. Fig. 2a was obtained with the same parameters, and thus shows the contours of H_{eff} for this parameter set. In our simulation, we made no other approximations than truncating the Hilbert space of the cavity to the first 650 photon number eigenstates (resulting in Hilbert space dimension 1300), and discretizing the Hamiltonian's continuous time-dependence within one period into 300 evenly spaced intervals.

We detected phase-locking from the distribution of level-spacings in the system's quasienergy spectrum $\{\varepsilon_n\}$.

The inset in Fig. 1c shows a histogram of the level spacings $\Delta\varepsilon_{mn} = \varepsilon_m - \varepsilon_n$ of the system, for all $1300 * 1299$ (ordered) pairs of quasienergy levels where $m \neq n$. The bin width in the histogram was chosen as $10^{-5}\Omega$, resulting in 10^5 bins. We thus expect the number of level pairs $N(\Delta\varepsilon)$ falling into the bin at level splitting $\Delta\varepsilon$ to be given by $1300^2/10^5 \approx 17$. While this estimate is accurate for almost all bins in Fig. 1c, there is an anomalously high (~ 100) number of level pairs in the spectrum whose splitting falls into the bin at $\Delta\varepsilon = \Omega/3$. From the discussion in Sec. II C, this indicates phase-locked motion in the model. Specifically, we expect the model supports approximately $100 - 17 \sim 85$ phase-locked Floquet eigenstates.

The above results suggest that we may use the histogram peak-height $N(\Delta\varepsilon = \Omega/3)$ to estimate the number of phase-locking Floquet states in the system. In the main panel of Fig. 1c, we plot this number as a function of the cavity frequency ω_c and coupling strength η, while keeping B_0 and A_d fixed at values 7 and 15, respectively. As is evident in Fig. 1c, period-3 phase-locking persists throughout parameter space, arising both for weak and strong detuning and nonlinearity. Thus, phase-locking is a generic and robust feature in periodically driven nonlinear quantum oscillators.

Focusing on the peak in Fig. 1c that emerges from $\omega_c = \Omega/3$, we see that, for $\eta \ll \Omega$, phase-locking occurs when $\omega_c \approx \Omega/3$. Interestingly, as η increases beyond $\Omega/2$, the cavity frequency interval at which phase locking occurs splits into two linearly-diverging branches when $\eta \gtrsim \Omega/2$. This point marks the crossover from the Floquet-locking regime (lower branch) to the adiabatic regime (upper branch): We recall from Sec. II B that the adiabatic regime arises when the *renormalized* oscillator frequency of the cavity matches a rational multiple of Ω: $\delta\omega \sim \mp\eta\kappa$. In contrast, the Floquet regime only arises when $\eta < \Omega$ and for small values of $\delta\omega$ (see Sec. II B 2). Thus, for fixed drive frequency Ω, the adiabatic regime gives rise to two branches of locking in parameter space at detuning $\delta\omega \propto \pm\eta$, while the Floquet regime gives rise to a single branch $\delta\omega \sim 0, \eta \ll \Omega$. This 3-pronged branch structure is clearly visible in Fig. 1c.

To further explore the signatures of quantum phase-locking, we computed the Wigner function $W(x, p)$ for each Floquet eigenstate $|\psi_n\rangle$, using the reduced density matrix of the cavity $\rho_{\text{cav}}^n = \text{Tr}_S[|\psi_n\rangle\langle\psi_n|]$, where Tr_S denotes the partial trace over the Hilbert space of the spin. We considered the two parameter sets used in Figs. 2ab, corresponding to the adiabatic and Floquet regimes (the former parameter set is also used for Fig. 1c).

In Fig. 3a, we show the Wigner function for a phase-locked Floquet eigenstate for the adiabatic regime parameters also used in Fig. 2a and Fig. 1c (i.e., we show one out of the set of many Floquet eigenstates whose quasienergies differ by an exact multiple of $\Omega/3$ from two other Floquet eigenstates in the system), see Sec. II B for parameters. The Wigner function of the phase-locked Floquet eigenstate in Fig. 3b shows a highly structured

pattern, with support only in 3 separate regions of phase space, related by rotation by approximately $2\pi/3$. The locations of the islands coincide with the locations of the minima in phase space of the corresponding effective Hamiltonian $H_{\mathrm{eff}}(x, p)$ in Fig. 2a (shown as grey lines in Fig. 3a), further validating the analytic discussion in Sec. II. In contrast to the phase-locked Floquet eigenstate shown in Fig. 3c, we show a typical (non-phase locked) Floquet eigenstate for this system. The Wigner function has most of its weight between cavity field amplitude $A_{\mathrm{cav}} = \sqrt{x^2 + p^2}$ values 12 and 22. Apart from this confinement, the Wigner function has no apparent structure, being evenly distributed with respect to phase, with a somewhat chaotic pattern.

We identified two other Floquet eigenstates of the system whose quasienergies differ by exactly $\pm\Omega/3$ from the quasienergy of the eigenstate depicted in Fig. 3b. The Wigner functions of these two other states are nearly identical to the Wigner function in Fig. 3a. According to the analysis in Sec. II C, we expect that these three $\Omega/3$-detuned Floquet eigenstates are of the form in Eq. (23), where $|\chi_m\rangle$ only has support within a particular "potential well" of $H_{\mathrm{eff}}(x, p)$ in Fig. 2a. We verified this hypothesis by computing the equal-weight linear combinations of the three Floquet eigenstates $\{|\Psi_\nu\rangle\}$, $\frac{1}{\sqrt{3}} \sum_{\nu=1}^{3} e^{2\pi i m\nu/3} |\Psi_\nu\rangle$ for $m = 1, 2, 3$. From Sec. II C, we expect the linear combination for each m to result in a state $|\chi_m\rangle$ which only has support in well m [see Eq. (23)]. This result is evident in Fig. 3d: here we show the Wigner function for the linear combination $|\chi_3\rangle$. In agreement with the discussion in Sec. II C, the Wigner function of $|\chi_3\rangle$ only has support in a single potential well of H_{eff} [namely near $(x, p) = (20, 0)$].

We also computed the Wigner functions of phase-locking Floquet eigenstates in the Floquet regime $\eta \ll \Omega, \delta\omega \sim 0$. In Fig. 3b, we plot the Wigner function of such a phase-locked Floquet eigenstate for the system with the parameters used in Fig. 2b. The Wigner functions of the phase-locked Floquet state exhibit very similar structure as in the adiabatic regime: there exist three islands where the Wigner function is nonzero and smoothly varying. The locations of these islands coincide with the locations of three symmetry-related local minima of the effective Hamiltonian of the system (see Fig. 2b). At the edges of the islands, the Wigner function exhibits oscillations from positive to negative whose nodal lines run along the contours of H_{eff}. The presence of these features hence strongly support the analytical discussion in Sec. II B 2.

In the Floquet regime, there are multiple extrema (minima and maxima) of H_{eff} that can support distinct families of phase-locked Floquet eigenstates. In Fig. 3e, we plot the Wigner function of a phase-locking Floquet eigenstate of the same system depicted in Fig. 3d, but with support near a distinct extremum of H_{eff} from the eigenstate depicted in Fig. 3b (note that only the first quadrant of phase space is shown). Moreover, each "potential well/peak" of H_{eff} may support several phase-
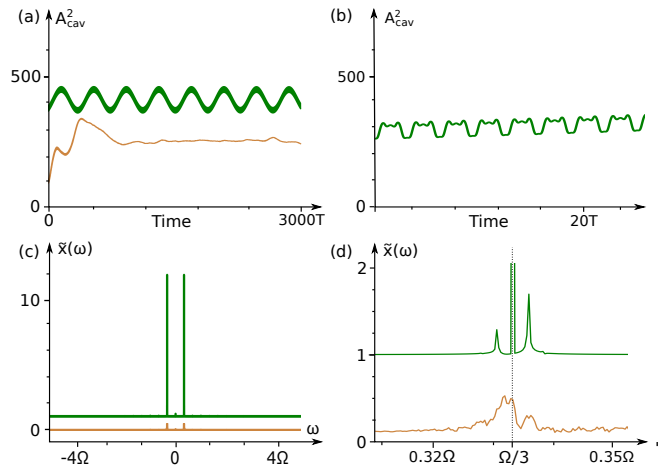

FIG. 4. Manifestations of phase-locking in the dynamics of the cavity-spin system considered in Sec. III. Green and orange curves indicate data for the system when initialized within, and outside the phase-locking regime, respectively (see main text for parameters and further details). (a) Evolution of squared field amplitude in cavity. (b) Zoom-in of panel (a) for the first 20 driving periods. (c) Frequency spectrum of the cavity observable $\langle \hat{x} \rangle$, with the green curve vertically offset by 1. (d) Zoom-in of panel (c), in the vicinity of $\omega = \Omega/3$ (indicated by vertical dashed line).

locking Floquet eigenstates. We illustrate this with Fig. 3f which shows another phase-locking Floquet eigenstate with support in the same potential well as the state depicted in Fig. 3e. These additional Floquet eigenstates can be seen as "excited states" of the potential wells.

To explore the physical manifestations of quantum phase locking, we considered the dynamics of cavity observables in the phase-locked regime, under the same parameters as used in the inset in Fig. 1c, Fig. 2a and Figs. 3ab. We computed the time-evolution of the system after initializing the cavity mode in a coherent state with phase 0 and displacement amplitude either 20 or 10, corresponding to locations $(x_0, p_0) = (20, 0)$ and $(x_0, p_0) = (10, 0)$ in phase-space. We initialized the spin in the state $|\downarrow\rangle$, anti-aligned with the initial effective magnetic field $\mathbf{b}(x_0, p_0, 0)$ for both initializations. From the effective cavity Hamiltonian of the system shown in Fig. 2a (for anti-aligned spin), we expect these two initializations to place the system inside and outside the phase-locking regime, respectively.

Figs. 4a-d show the evolution and frequency spectra of various quantities for these two initializations. Here green and orange curves correspond to the initializations with $x_0 = 20$ and $x_0 = 10$, respectively. In Fig. 4a, we show the evolution of the squared cavity amplitude A_{cav}^2 for the first 3000 driving periods for both initializations. Fig. 4b shows a zoom-in of the same data for the first 20 periods. In the phase-locked regime (green), A_{cav}^2 undergoes a slow modulation of periodicity $\sim 380T$. This modulation arises from the wave-packet of the system precessing around the minimum of H_{eff} in the rotating

frame (see Sec. II C). In addition to this slow modulation, the cavity mode exhibits a rapid oscillation with periodicity $3T$, which is clearly visible in Fig. 4b. In contrast, when the system is initialized outside the phase-locking regime (orange), the cavity does not oscillate with well-defined periodicity.

The phase-locking is particularly clear in the frequency spectrum of cavity observables. Fig. 4c shows the dimensionless Fourier transform of $\langle \hat{x}(t) \rangle$ (absolute value) $|\tilde{x}(\omega)|$ for the two initializations above[67], while Fig. 4d shows a close-up of the spectrum near $\omega_c = \Omega/3$. In the phase-locking regime, $|\tilde{x}(\omega)|$ features an extremely sharp peak of magnitude ~ 10 at $\omega = \Omega/3$. The two side-peaks visible in Fig. 4d arise from the slow modulation of the cavity state discussed above: Their offset from the main peak defines the oscillation frequency of the cavity wave-packet around the local minimum of H_{eff}. As is evident in Figs. 4cd, the system has a clear, measurable subharmonic response to the driving in the phase-locked regime. In contrast, outside the phase-locking regime (orange), the frequency spectrum of x shows a broad feature around the same value, but no well-defined peak.

IV. DISCUSSION

The discovery of Floquet time crystals sparked a broader investigation of discrete time-translation symmetry breaking phenomena. In this paper, we showed how such symmetry breaking emerges in a periodically driven spin-cavity system. Using a semiclassical phase-space approach along with the framework of Floquet states and quasienergies, we identified two mechanisms for phase locking, which allow this phenomenon to occur in a wide region of parameter space. In these phase-locked regimes, the system exhibits well-defined oscillations, with extended period qT, where T denotes the period of the driving field, and q is an integer. This phase-locking does not require any fine-tuning, but emerges for a finite range of detuning $\delta\omega = \omega_c - r\Omega/q$, and for both weak and strong qubit-cavity coupling η.

Quantum phase-locking has remarkable consequences for the quasienergy spectrum of the system. In the phase-locked regime, a large number of multiplets of Floquet eigenstates emerge whose quasi-energy differences are exponentially close to $n\Omega/q$ for $n = 1, \ldots, q$. This multiplicity is remarkable; for comparison, time-crystalline behavior in spin chains (see, e.g., Refs. 11 and 12) is also manifested in a large degeneracy of period-doubled Floquet eigenstates. However, for these systems, period multiplication emerges from the many-body nature of the system, which is fundamentally different mechanism from the case we considered here. For Floquet crys-

tals, each quasienergy level in the system forms a part of a phase-locking multiplet. In contrast, for the qubit-cavity system we study here, only a finite number of quasienergy levels form multiplets. However, the phase-locking regime we describe still takes up a finite volume of phase and parameter space, and can be reached through appropriately controlled but not fine-tuned initialization of the cavity mode.

The driven spin-cavity system we considered is perhaps one of the simplest systems that exhibits quantum phase-locking. This generic class of models arise in a diverse range of settings and physical systems, and can for instance describe Rydberg atoms in optical cavities, as well as qubits in contact with microwave modes. Due to the simplicity of the model, and the many suitable experimental platforms, we expect that the qubit-cavity model forms a convenient and versatile platform for studying the breakdown of time-translation symmetry.

We expect that the nontrivial fixed points of the stroboscopic motion generated by H_{eff} remain stable in the presence of weak dissipation in the cavity, as would be the case if the radiation is allowed to leak out. In this case the phase-locking effect could be used for extracting an output signal whose frequency is given by a rational fraction of the drive, thus achieving frequency conversion. This offers an interesting direction for future studies.

At strong coupling η, phase-locking coexists with the topological energy-pumping regime that was analyzed in Ref. 14. Thus, the relatively simple and experimentally accessible model of a driven qubit-cavity system supports several distinct, highly nontrivial non-equilibrium phenomena. The simplicity of the platform, and the interplay of these nontrivial phenomena makes the driven qubit-cavity system an interesting subject for future experimental and theoretical studies.

Other interesting subjects for future study include the fate of phase-locking in the presence of multiple cavity modes with different frequencies, and the nature of the transition between the Floquet and adiabatic regimes. A question of particular interest is whether the splitting of the period multiplication branch in Fig. 1c is a dynamical system bifurcation, or whether the splitting has a different origin.

[1] J. Dalibard, F. Gerbier, G. Juzeliūnas, and P. Öhberg, Rev. Mod. Phys. **83**, 1523 (2011).

[2] A. Eckardt, Rev. Mod. Phys. **89**, 011004 (2017).

[3] N. R. Cooper, J. Dalibard, and I. B. Spielman, Rev. Mod. Phys. **91**, 015005 (2019).

[4] T. Oka and S. Kitamura, Annual Review of Condensed Matter Physics **10**, 387 (2019).

[5] M. S. Rudner and N. H. Lindner (2019), 1909.02008.

[6] F. Harper, R. Roy, M. S. Rudner, and S. L. Sondhi (2019), 1905.01317.

[7] T. Kitagawa, E. Berg, M. Rudner, and E. Demler, Phys. Rev. B **82**, 235114 (2010).

[8] L. Jiang, T. Kitagawa, J. Alicea, A. R. Akhmerov, D. Pekker, G. Refael, J. I. Cirac, E. Demler, M. D. Lukin, and P. Zoller, Phys. Rev. Lett. **106**, 220402 (2011).

[9] M. S. Rudner, N. H. Lindner, E. Berg, and M. Levin, Phys. Rev. X **3**, 031005 (2013).

[10] P. Titum, E. Berg, M. S. Rudner, G. Refael, and N. H. Lindner, Phys. Rev. X **6**, 021013 (2016).

[11] V. Khemani, A. Lazarides, R. Moessner, and S. L. Sondhi, Phys. Rev. Lett. **116**, 250401 (2016).

[12] D. V. Else, B. Bauer, and C. Nayak, Phys. Rev. Lett. **117**, 090402 (2016).

[13] I. Martin, G. Refael, and B. Halperin, Phys. Rev. X **7**, 041008 (2017).

[14] F. Nathan, I. Martin, and G. Refael, Physical Review B **99** (2019).

[15] M. H. Kolodrubetz, F. Nathan, S. Gazit, T. Morimoto, and J. E. Moore, Phys. Rev. Lett. **120**, 150601 (2018).

[16] F. Nathan, D. Abanin, E. Berg, N. H. Lindner, and M. S. Rudner, Physical Review B **99** (2019).

[17] A. Chandran and S. L. Sondhi, Phys. Rev. B **93**, 174305 (2016).

[18] H. C. Po, L. Fidkowski, T. Morimoto, A. C. Potter, and A. Vishwanath, Physical Review X **6**, 041070 (2016).

[19] D. Reiss, F. Harper, and R. Roy, Phys. Rev. B **98**, 045127 (2018).

[20] A. C. Potter, A. Vishwanath, and L. Fidkowski, Phys. Rev. B **97**, 245106 (2018).

[21] N. Yao, A. Potter, I.-D. Potirniche, and A. Vishwanath, Physical Review Letters **118** (2017), ISSN 1079-7114.

[22] D. V. Else, B. Bauer, and C. Nayak, Physical Review X **7**, 011026 (2017).

[23] F. Iemini, A. Russomanno, J. Keeling, M. Schirò, M. Dalmonte, and R. Fazio, Phys. Rev. Lett. **121**, 035301 (2018).

[24] P. Nurwantoro, R. Weda Bomantara, and J. Gong, arXiv e-prints arXiv:1909.04337 (2019).

[25] V. Khemani, C. W. von Keyserlingk, and S. L. Sondhi, Phys. Rev. B **96**, 115127 (2017).

[26] R. Moessner and S. L. Sondhi, Nature Physics **13**, 424 (2017).

[27] V. Khemani, A. Lazarides, R. Moessner, and S. L. Sondhi, Phys. Rev. Lett. **116**, 250401 (2016).

[28] B. Huang, Y.-H. Wu, and W. V. Liu, Phys. Rev. Lett. **120**, 110603 (2018).

[29] M. Holthaus and M. E. Flatté, Physics Letters A **187**, 151 (1994), ISSN 0375-9601.

[30] Y. Zhang, J. Gosner, S. M. Girvin, J. Ankerhold, and M. I. Dykman, Phys. Rev. A **96**, 052124 (2017).

[31] S. Autti, V. B. Eltsov, and G. E. Volovik, Phys. Rev. Lett. **120**, 215301 (2018).

[32] L. Bello, M. Calvanese Strinati, E. G. Dalla Torre, and A. Pe'er, Phys. Rev. Lett. **123**, 083901 (2019).

[33] J. G. Cosme, J. Skulte, and L. Mathey, arXiv e-prints arXiv:1909.00266 (2019).

[34] B. Zhu, J. Marino, N. Y Yao, M. D. Lukin, and E. A. Demler, New Journal of Physics **21**, 073028 (2019).

[35] Z. Gong, R. Hamazaki, and M. Ueda, Phys. Rev. Lett. **120**, 040404 (2018).

[36] D. Barberena, R. J. Lewis-Swan, J. K. Thompson, and A. M. Rey, Phys. Rev. A **99**, 053411 (2019).

[37] M. A. Broome, A. Fedrizzi, B. P. Lanyon, I. Kassal, A. Aspuru-Guzik, and A. G. White, Phys. Rev. Lett. **104**, 153602 (2010).

[38] G. Jotzu, M. Messer, R. Desbuquois, M. Lebrat, T. Uehlinger, D. Greif, and T. Esslinger, Nature **515**, 237 (2014).

[39] W. Hu, J. C. Pillay, K. Wu, M. Pasek, P. P. Shum, and Y. D. Chong, Phys. Rev. X **5**, 011012 (2015).

[40] J. Zhang, P. W. Hess, A. Kyprianidis, P. Becker, A. Lee, J. Smith, G. Pagano, I.-D. Potirniche, A. C. Potter, A. Vishwanath, et al., Nature **543**, 217 (2017).

[41] L. J. Maczewsky, J. M. Zeuner, S. Nolte, and A. Szameit, Nature Comm. **8**, 13756 (2017).

[42] S. Mukherjee, A. Spracklen, M. Valiente, E. Andersson, O. Ohberg, N. Goldman, and R. R. Thomson, Nature Comm. **8**, 13918 (2017).

[43] J. W. McIver, B. Schulte, F.-U. Stein, T. Matsuyama, G. Jotzu, G. Meier, and A. Cavalleri, Nature Physics (2019).

[44] J. Zhang, P. W. Hess, A. Kyprianidis, P. Becker, A. Lee, J. Smith, G. Pagano, I. D. Potirniche, A. C. Potter, A. Vishwanath, et al., Nature **543**, 217 (2017).

[45] J. Choi, H. Zhou, S. Choi, R. Landig, W. W. Ho, J. Isoya, F. Jelezko, S. Onoda, H. Sumiya, D. A. Abanin, et al., Phys. Rev. Lett. **122**, 043603 (2019).

[46] K. Wintersperger, C. Braun, F. N. Ünal, A. Eckardt, M. D. Liberto, N. Goldman, I. Bloch, and M. Aidelsburger (2020), 2002.09840.

[47] C. Gross and I. Bloch, Science **357**, 995 (2017), ISSN 0036-8075.

[48] G. Burkard, M. J. Gullans, X. Mi, and J. R. Petta, Nature Reviews Physics **2**, 129 (2020).

[49] A. A. Clerk, K. W. Lehnert, P. Bertet, J. R. Petta, and Y. Nakamura, Nature Physics **16**, 257 (2020).

[50] S. N. Rasband, *Chaotic Dynamics of Nonlinear Systems* (John Wiley and Sons, 1990).

[51] S. Strogatz, *Nonlinear Dynamics And Chaos: With Applications To Physics, Biology, Chemistry, And Engineering (Studies in Nonlinearity)* (Westview Press, 2001).

[52] M. R. Jessop, W. Li, and A. D. Armour, arXiv e-prints arXiv:1906.07603 (2019).

[53] J. Tan and G. Gabrielse, Phys. Rev. Lett. **67**, 3090 (1991).

[54] N. Lörch, Y. Zhang, C. Bruder, and M. I. Dykman, Physical Review Research **1** (2019), ISSN 2643-1564.

[55] Here, and throughout, we work in units where $\hbar = 1$.

[56] Note that x and p are normalized such that $\frac{1}{2}(\hat{x}^2 + \hat{p}^2)$ gives the number of photons in the cavity mode.

[57] V. E. Manucharyan, J. Koch, L. I. Glazman, and M. H. Devoret, Science **326**, 113 (2009).

[58] L. B. Nguyen, Y.-H. Lin, A. Somoroff, R. Mencia, N. Grabon, and V. E. Manucharyan, Phys. Rev. X **9**, 041041 (2019).

[59] L. Childress, M. V. G. Dutt, J. M. Taylor, A. S. Zibrov, F. Jelezko, J. Wrachtrup, P. R. Hemmer, and M. D. Lukin, Science **314**, 281 (2006).

[60] A. O. Sushkov, I. Lovchinsky, N. Chisholm, R. L. Walsworth, H. Park, and M. D. Lukin, Phys. Rev. Lett. **113**, 197601 (2014).

[61] G. Bentsen, I.-D. Potirniche, V. B. Bulchandani, T. Scaf-

fidi, X. Cao, X.-L. Qi, M. Schleier-Smith, and E. Altman, Phys. Rev. X **9**, 041011 (2019).

[62] R. M. Kroeze, Y. Guo, V. D. Vaidya, J. Keeling, and B. L. Lev, Phys. Rev. Lett. **121**, 163601 (2018).

[63] Note that H_{eff} is not uniquely defined for the system, due to the periodic nature of the quasienergies.

[64] We note there exists some non-typical cases where the stated conditions for adiabatic locking are not sufficient. See Appendix C for discussion and rigorous conditions.

[65] This follows when using $\partial_p|\mathbf{h}| = \partial_p\mathbf{h}\cdot\mathbf{n}$, where $\mathbf{n} = \mathbf{h}/|\mathbf{h}|$. The quoted result then follows since $|\mathbf{n}| = |\partial_p\mathbf{h}| = 1$ [see below Eq. (11)].

[66] P. Weinberg, M. Bukov, L. D'Alessio, A. Polkovnikov, S. Vajna, and M. Kolodrubetz, Physics Reports **688**, 1 (2017), ISSN 0370-1573, adiabatic Perturbation Theory and Geometry of Periodically-Driven Systems.

[67] Here $\tilde{x}(\omega) \equiv \lim_{\tau\to\infty}\frac{1}{\tau}\int_0^\tau \mathrm{d}t\, e^{i\omega t}x(t)$ denotes the Fourier transform of $x(t)$. The data in Fig. 4cd are computed using $\tau = 3000T$.

[68] Specifically, the inherent structure of H_F implies that terms in Eq. (A4) can only be nonzero if $r(m-n) = lq$ for some integer l. Since q/r is an irreducible fraction, this can only be true if $l = rk$ for some integer k. As a result, sites m and n are coupled only when $m - n = kq$.

[69] A. Altland and M. R. Zirnbauer, Phys. Rev. B **55**, 1142 (1997).

Appendix A: Photon lattice picture of phase locking

In this appendix, we present a complementary perspective of phase locking, based on the photon lattice picture of periodically driven systems. The approach is used to analyze the emergence of phase-locking of the cavity-qubit model, in the limit of small anharmonicity η and detuning. To demonstrate the emergence of phase-locking, we consider the case where the driving frequency is close to a rational multiple of the cavity frequency, $\Omega \approx q\omega_c/r$, where q and r are integers. We analyze the model as a periodically driven system with driving period $qT = 2\pi q/\Omega$ [recall that $H(t) = H(t+T)$ implies $H(t) = H(t+qT)$].

For a periodically driven system with driving period qT, the photon lattice Hilbert space is spanned by the orthonormal basis $|i, n_d\rangle\!\rangle = |i\rangle \otimes |n_d\rangle$, where i indexes the basis states of the original problem, while $n_d \in \mathbb{Z}$ can be seen as a lattice index, and heuristically counts the number of drive photons with energy $2\pi/qT$. The extended Hilbert space Hamiltonian reads $H_F = \frac{2\pi}{qT}\hat{n}_d + \sum_{z,w} H_{ij}^z |i, w+z\rangle\!\rangle\langle\!\langle j, w|$, where $\hat{n}_d|i,n\rangle\!\rangle = n|i,n\rangle\!\rangle$, and H_{ij}^z denotes the Fourier coefficients of $H_{ij}(t)$ (as a qT-periodic function of time). One can verify that the eigenstates of H_F, $|\psi_n\rangle\!\rangle = \sum_{i,z}\psi_{i,z}^n|i,z\rangle\!\rangle$, are related to the Floquet eigenstates of $H(t)$ as follows:

$$|\psi_n\rangle = \sum_{i,z}\psi_{i,z}^n|i\rangle. \tag{A1}$$

The quasienergy of the state $|\psi_n\rangle$ is related to the corresponding energy as $\varepsilon_n = E_n \pmod{2\pi/qT}$. Note that
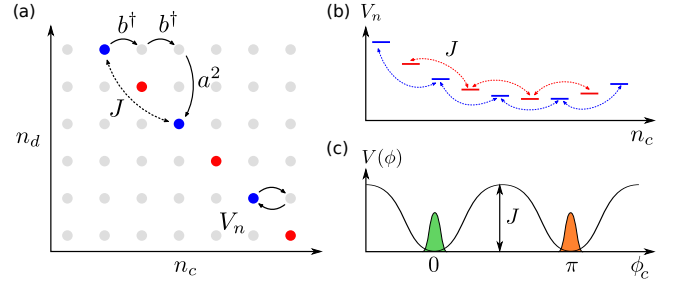

FIG. 5. Photon lattice representation of phase locking when drive Ω is close to $2\omega_c$. (a) Photon lattice of the system (see main text for details). Red and blue indicates the chain of sites along which the eigenstates of H_F have their primary support when $\Omega \approx 2\omega_c$. Arrows indicate examples of resonant virtual processes contributing to the second nearest-neighbour tunneling J and on-site potential V_n of the effective tight-binding Hamiltonians of the chain. Different colors emphasize the decoupling into independent sublattices. (b) Schematic depiction of a tight-binding Hamiltonian for the chains, with sites and on-site potential shown as a function of n_c. (c) Energy profile as a function of the oscillator phase ϕ_c (variable conjugate to n_c), for the oscillator states close to the minimum of V_n. Green and orange are approximate bound states of the effective Hamiltonian near $\phi_c = 0$ and π, each a superposition of "red" and "blue" chain states in (b). Up to exponentially weak tunneling correction, these bound states are also Floquet eigenstates, corresponding to the semiclassical states with with the oscillator phases locked to 0 or π respectively.

each Floquet eigenstate of $H(t)$ corresponds to an infinite family of eigenstates of H_F due to the symmetry $[\hat{a}, H_F] = \frac{2\pi}{qT}$, where $\hat{a}|i, n_d\rangle\!\rangle = |i, n_d - 1\rangle\!\rangle$. As a result, if $|\psi_n\rangle\!\rangle$ is an eigenstate of H_F with energy E_n, $\hat{a}|\psi_n\rangle\!\rangle$ is also an eigenstate of H_F, with energy $E_n - 2\pi/(qT)$. Both eigenstates correspond to the same Floquet eigenstate through Eq. (A1).

To find H_F for the cavity-qubit system, we recall that the Hilbert space of the system is spanned by the states $|\alpha n_c\rangle$, where $n_c = 0, 1, \ldots$ counts the number of cavity photons, while $\alpha = 1, 2$ denotes the state of the qubit. Hence, we can label the basis states for the extended Hilbert space $|\alpha, n_c, n_d\rangle\!\rangle = |\alpha, n_c\rangle \otimes |n_d\rangle$. We write $H_F = V + K$ where V and K denote the diagonal and off-diagonal components in the basis above. To find V and K, we recall from Eqs. (1)-(5) in the main text that the Hamiltonian $H(t)$ oscillates monochromatically with period T. Therefore, H_{ij}^z is nonzero only when z is an integer multiple of q. Equivalently, the above-introduced photon number shift operators $\hat{a}$ and $\hat{a}^\dagger$ only appear in powers of q in the expression for H_F. Using the expression for $H(t)$ in Eqs. (1)-(5), we find

$$V = \hat{n}_c\omega_c + \frac{\Omega}{q}\hat{n}_d + \eta\sigma_x B_0 \tag{A2}$$

$$K = \frac{\eta A_d}{2}\left(\hat{a}^q[\sigma_z - i\sigma_x] + \hat{a}^{\dagger q}[\sigma_z + i\sigma_x]\right) + \eta(\hat{b}\sigma^+ + \hat{b}^\dagger\sigma^-).$$

In the same way as for example in Refs. 13 and 14,

we can see H_F as describing a $2D$ square lattice tight-binding model where (n_c, n_d) denotes the site index in the "photon" lattice, and α denotes the orbital index. The sites in the photon lattice are coupled by the term K, and are subject to the on-site potential energy term V. Note that, by construction, the Hamiltonian $H_F = V + K$ only couples sites (n_c, n_d) in the photon lattice separated by a distance q in the second coordinate.

In the limit $\eta \to 0$, the term V will generally dominate, and the eigenstates of H_F are localized on individual sites in the photon lattice. The eigenstates are given by $|\Psi_{mn}^{\pm}\rangle\rangle \approx \frac{1}{\sqrt{2}}(|1, m, n\rangle\rangle \pm |2, m, n\rangle\rangle)$, with energies

$$E_{mn}^{\pm} = m\omega_c + \frac{n\Omega}{q} \pm \eta B_0. \qquad (A3)$$

These solutions are trivial, and hence typically there is no phase-locking in the small-η limit.

However, when the driving frequency Ω is sufficiently close to $\omega_c q/r$, there is an exception to the above result. In this case, the "potential energies" on sites (n_c, n_d) and $(n_c + 1, n_d - r)$ can be close enough that the term K couples these sites resonantly through a high-order virtual processes. As a result, each eigenstate of H_F may extend along a chain of sites $(k, b - rk)$ for $k = 0, 1, \ldots$, as depicted in Fig. 5a for the case $q/r = 2$. Due to the symmetry of H_F described below Eq. (A1), there is just one independent chain $(b = 0)$, while the remaining chains are related by shifts in n_d.

Each chain is subject to an effective Hamiltonian which arises from the high-order virtual processes. This Hamiltonian takes the form

$$H_{\text{eff}} = \sum_{m,n} |\alpha, m, -rm\rangle\rangle\langle\langle\beta, n, -rn| H_{mn}^{\alpha\beta}. \qquad (A4)$$

Here the matrix elements $H_{mn}^{\alpha\beta}$ can in principle be calculated analytically from perturbation theory in η. Since H_F by construction only couples sites (n_c, n_d) in the photon lattice separated by a distance q in the second coordinate, the terms off-diagonal in photon number basis can only be nonzero when $m - n = kq$ for some integer k[68].

The above considerations show that the 1D chain model above itself separates into q decoupled sublattices, distinguished by the value of $n_c \pmod q$. The tunneling coefficient $H_{m,m+kq}^{\alpha\beta}$ arises from a $k(q + r)$-th order virtual process (see Fig. 5a), and hence scales as $\eta^{k(q+r)}$. Thus, only the $k = 1$ term is relevant in the $\eta \to 0$ limit. Following this discussion, we conclude that $H_{mn}^{\alpha\beta}$ takes the form

$$H_{mn} = V_n \delta_{mn} + \frac{1}{2}(J_n \delta_{m,n+q} + J_n^{\dagger} \delta_{n+q,m}) \qquad (A5)$$

where V_n and J_n are 2×2 matrices acting on the Hilbert space of the qubit, and we suppressed the qubit indices α, β for brevity. The term V_n has contributions from the static field B_0, from the finite detuning $\delta\omega$, and from even-order "closed" virtual processes, while the origin of the term J_n was discussed in the above.

While it is straightforward to analytically compute the terms V_n and J_n above through perturbation theory in η, such an analysis is beyond the scope of this paper. Instead, below we infer the emergence of phase-locking from a more qualitative discussion of the effective Hamiltonian above. We consider the case of a spinless model, where the coefficients V_n and J_n in Eq. (A5) are scalars. Such a Hamiltonian emerges when the above line of arguments is applied to a periodically-driven anharmonic oscillator, such as considered in Ref. 30. We expect that the "spinful" model arising from the cavity-qubit system can be analyzed in a similar way.

To see how phase-locking arises in the spinless model, we note that for a finite range of detuning $\delta\omega = \omega - r\Omega/q$ the net potential energy $\tilde{V}_n = V_n + |J_n|$ may have a nontrivial minimum as a function of n, as schematically illustrated in Fig. 5c (the case of a maximum is similar). Near the minimum n_0 of $\tilde{V}_n$, to lowest order in $n - n_0$, H takes the form

$$H_{mn} \approx \frac{k}{2}(n - n_0)^2 \delta_{mn} + \frac{J}{2}(\delta_{m,n+q} + \delta_{m,n-q} - 2), \quad (A6)$$

where $J = J_{n_0}$, and the "spring constant" k can be computed from Taylor expanding $\tilde{V}_n$ around $n = n_0$. It is illuminating to express the Hamiltonian above in terms of the variable ϕ conjugate to $n - n_0$:

$$H_{\text{eff}} = -\frac{1}{2m_{\text{eff}}}\partial_\phi^2 + J(\cos(q\phi) - 1), \qquad (A7)$$

where $m_{\text{eff}} = 1/k$. Physically, since the index n measures the value of $\hat{n}_c$ (i.e. the number of cavity mode photons) up to a constant shift by n_0 [see Eq. (A4)], ϕ measures the phase of the cavity mode. Thus, when $n_c \approx n_0$ the effective Hamiltonian for the phase of the cavity mode describes the Hamiltonian of a free particle in a cosine potential $V(\phi)$ with well spacing $2\pi/q$ and depth J, as depicted in Fig. 5c.

Importantly, when the potential well depth J is sufficiently large compared to the of kinetic energy of zero-point fluctuations associated with the effective mass m_{eff}, the effective Hamiltonian above may support bound states where wave function of the system (as a function of ϕ) is confined to one of the potential wells. In this state, with exponential accuracy, the phase of the oscillator ϕ is locked to an integer multiple of $2\pi/q$.

We now demonstrate that these bound states can be used to construct Floquet eigenstates of the cavity-qubit model where the phase has locked to the driving field [recall that the eigenstates in the photon lattice correspond to Floquet eigenstates of the cavity-qubit system through Eq. (A1)]. Indeed, from the bound states $|\psi_z\rangle\rangle$ localized in isolated potential wells z, one can construct plane-wave" combinations, $|\Psi_n\rangle\rangle = \frac{1}{\sqrt{q}}\sum_z |\psi_z\rangle\rangle e^{-\frac{2\pi i z n}{q}}$. Due to gaussian confinement of the wavefunction in the bottom of the near-harmonic potential wells in Eq. (A7), the energy differences between these distinct combinations will be exponentially small in λ^2/ξ^2, where $\lambda = 2\pi/q$ denotes the well separation, and $\xi = (Jm_{\text{eff}})^{-1/4}$ denotes

the scale of the phase fluctuations around the potential minimum.

Through the correspondence between eigenstates of H_F and the Floquet eigenstates of the system, we conclude there must exist families of q Floquet eigenstates, whose quasienergies differ by an integer multiple of Ω/q, up to a correction $\delta\varepsilon$ exponentially small in $\lambda^2/\xi^2 \sim \sqrt{Jm_{\text{eff}}}/q^2$. This is in agreement with the main text, where we indeed found multiplets of Floquet eigenstates with exponentially close quasienergies modulo Ω/q.

Appendix B: Phase locking at other frequency ratios

Here we demonstrate in numerics that the phase locking can also occur at ratios other than 3. For the same model and realizations studied in Sec. III (see Fig. 1c), we counted the number of phase-locking Floquet eigenstates at period multiplication q for $q = 2, 4, 5, 6$, as a function of the coupling strength η and cavity frequency ω_c. The phase-locking states were identified from the quasienergy level spacings (modulo Ω/q), in the same way as for the period-3 phase locking states (see Sec. III for more details). Our counting procedure identified a unique period multiplication for each phase-locking state, such that period-2 phase-locking eigenstates were not also double-counted as a period-4 Floquet eigenstates. In Fig. 6, we plot the number of period-q phase-locking states for $q = 2, 4, 5, 6$, as a function of the cavity-qubit coupling η and cavity frequency ω_c. Note that a different color scale is used compared to Fig. 1, in order to heighten the contrast.

Fig. 6 clearly shows the same branch structure as Fig. 1c, with period-q phase-locking occurring whenever ω_c/Ω is close to r/q for integer r. This shows that period-q phase locking can occur for any q (when ω_c/Ω is close enough to r/q for some integer r).

Appendix C: Adiabatic and Floquet regimes

In this subsection, we derive the conditions for adiabatic and Floquet regimes quoted in Secs. II B and II B 2. We also derive the expression in Eqs. (19) and (20) for the effective Hamiltonian in the Floquet regime.

1. Adiabatic regime

Here we identify the conditions where the spin is locked to the direction of the instantaneous field $\mathbf{h}(x, p, t)$ [see Eq. (11)] due the time-dependence of $\mathbf{h}(x, p, t)$ being adiabatic. These conditions were conditions quoted below Eq. (15) in the main text

As discussed above Eq. (12) in the main text, the time-dependence of $\mathbf{h}(x, p, t)$ is adiabatic when

$$\left| \frac{d}{dt} \frac{\mathbf{h}(x, p, t)}{|\mathbf{h}(x, p, t)|} \right| \ll \eta |\mathbf{h}(x, p, t)|, \tag{C1}$$

where the time-derivative includes the contributions from the motion of the cavity variables x and p: $\frac{d}{dt}\mathbf{h} = \partial_x \mathbf{h} \dot{x} + \partial_p \mathbf{h} \dot{p} + \partial_t \mathbf{h}$. As a first step, we note that, for any vector $\mathbf{v}(x)$, $|\partial_x(\mathbf{v}/|\mathbf{v}|)| \leq |\partial_x \mathbf{v}|/|\mathbf{v}|$. Thus, it is sufficient to identify the conditions where

$$|\partial_x \mathbf{h} \dot{x}| + |\partial_p \mathbf{h} \dot{p}| + |\partial_t \mathbf{h}| \ll \eta |\mathbf{h}|^2. \tag{C2}$$

We first consider the last term in the above left hand side. From the definition of $\mathbf{h}(x, p, t)$ below Eq. (8) [see also Eq. (7)], we find $|\partial_t \mathbf{h}| \leq \Omega(A_{\text{cav}} + A_d)$, where $A_{\text{cav}} = \sqrt{x^2 + p^2}$ denotes the amplitude of the cavity field, and we used $\tilde{\Omega} \leq \Omega$. Moreover, we recall that $|\partial_x \mathbf{h}| = |\partial_p \mathbf{h}| = 1$. Finally, we note from Eqs. (9) and (10) that $|\dot{x}|, |\dot{p}| \leq \Omega A_{\text{cav}} + \eta$, where we used $|\delta\omega| \lesssim \Omega$. Using these inequalities in the expression above, we find that the time-dependence of $\mathbf{h}$ is adiabatic when

$$\Omega(A_d + 3A_{\text{cav}}) + 2\eta A_{\text{cav}} \ll \eta |\mathbf{h}|^2. \tag{C3}$$

To get a more convenient expression for the condition above, we note that, from the definition of $\mathbf{h}$, $A_d, A_{\text{cav}} \lesssim |\mathbf{h}|$. Using this estimate along with $\tilde{\Omega} \sim \Omega$ and $\Omega \gtrsim \delta\omega$, we conclude that the adiabatic regime generally arises if $4\Omega|\mathbf{h}| + 2\eta \ll |\mathbf{h}|^2 \eta$. This condition can be summarized by requiring that the following two conditions must be met:

$$|\mathbf{h}(x, p, t)| \gg \Omega/\eta, 1. \tag{C4}$$

This was the result we quoted below Eq. (15).

2. Floquet regime

Here establish the conditions for the Floquet regime quoted in the main text [Eq. (21)], and derive the effective Hamiltonian in Eq. (19).

a. Conditions for the Floquet regime

Here we derive the conditions for the Floquet regime. We first establish the conditions for integrating out the spin, and subsequently identify the conditions under which the time-dependence of $\mathbf{h}$ may be integrated out.

As quoted in Sec. II B 2 (see also Ref. 66), the trajectory of the spin $\mathbf{S}(t)$ is locked to $\mathbf{n}_0(x(t), p(t), t)$ when the change of the stroboscopic rotation axis $\mathbf{a}(x, p) = \mathbf{n}_0(x, p, 0)$ (due to the motion of x and p) is adiabatic with respect to the quasienergy gap $\delta\varepsilon(x, p) = \min(\varepsilon(x, p), \tilde{\Omega} - \varepsilon(x, p))$ (see sec. II B 2 for definition):

$$\left| \frac{d}{dt} \mathbf{a}(x(t), p(t)) \right| \ll \delta\varepsilon(x(t), p(t)), \tag{C5}$$

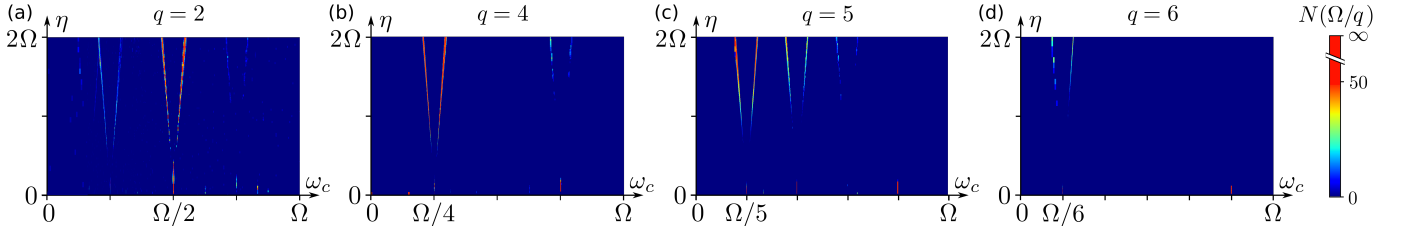FIG. 6. Number of period-q phase locking Floquet eigenstates as a function of ω_c and η, for the model depicted in Fig. 1c, for $q = 2$ (a), $q = 4$ (b), $q = 5$ (c), and $q = 6$(d). See Appendix B for further details.

where (with x, p, and t suppressed)

$$\frac{d}{dt}\mathbf{a} = \dot{x}\partial_x\mathbf{a} + \dot{p}\partial_p\mathbf{a}. \tag{C6}$$

To identify the conditions under which the inequality (C5) holds, we thus need to compute the x- and p-derivatives of the stroboscopic rotation axis $\mathbf{a}(x, p)$.

To relate $\mathbf{a}(x, p)$ to the field $\mathbf{h}(x, p, t)$, we consider the spin's dynamics [Eq. (11) in the main text] for fixed x and p. In this case $\mathbf{S}(t)$ evolves according to the Schrödinger-type equation

$$\partial_t S_k(t) = -i\sum_l H^{(3)}_{kl}(x, p, t)\mathbf{S}_l(t), \tag{C7}$$

where $H^{(3)}_{kl}(x, p, t) = -i\eta\sum_j h_j(x, p, t)\epsilon_{jkl}$ is a 3×3 Hermitian matrix, with ϵ_{jkl} denoting the Levi-Civita tensor. Due to the Floquet theorem, the equation of motion above has 3 complex-valued orthonormal solutions of the form $\mathbf{S}(t) = \mathbf{n}_j(t)e^{-i\varepsilon_j t}$, where $\mathbf{n}_j(t) = \mathbf{n}_j(t + qT)$. The antisymmetry of $H^{(3)}(t)$ (class D in the AZ classification[69]) implies that one of the stationary solutions is real-valued, with quasienergy zero. We identify this solution as the vector $\mathbf{n}_0(x, p, t)$ from Sec. II B 2. Up to a prefactor, $\mathbf{n}_0(x, p, t)$ is the unique qT-periodic solution to Eq. (11), with x and p fixed. The remaining two orthogonal solutions are related to each other by Hermitian conjugation, and have quasienergies $\pm\varepsilon_0(x, p)$. The above properties imply that the effective Hamiltonian associated with $H^{(3)}(x, p, t)$ is given by

$$H^{\text{spin}}_{\text{eff}}(x, p) = \varepsilon_0(x, p)\mathbf{a}(x, p)\cdot\mathbf{S}, \tag{C8}$$

where we used $\mathbf{n}_0(x, p, t) = \mathbf{a}(x, p)$. Comparing with the expression for $H^{\text{spin}}_{\text{eff}}(x, p)$ in Sec. II B 2, we conclude $\varepsilon_0(x, p) = \varepsilon(x, p)$. Thus, we have related $\mathbf{a}(x, p)$, $\mathbf{n}_0(x, p, t)$ and $\varepsilon(x, p)$ to the Floquet states and quasienergy spectrum of the 3×3 antisymmetric Hamiltonian $H^{(3)}(x, p, t)$.

To obtain a bound for $\partial_x\mathbf{a}$, we consider the Floquet operator $R(x, p, qT)$, where $R(x, p, t) \equiv \mathcal{T}e^{-i\int_0^t dt'\, H^{(3)}(x,p,t')}$ denotes the time-evolution operator generated by $H^{(3)}(x, p, t)$. Due to the antisymmetry of $H^{(3)}(x, p, t)$, $R(x, p, t)$ is an orthogonal matrix. Standard perturbative arguments (see below) show that

$$|\partial_x\mathbf{a}| \leq \frac{2\|\partial_x R(qT)\|}{\pi\delta\varepsilon(x, p)qT}, \tag{C9}$$

where $\|\cdot\|$ refers to the spectral norm.

To prove Eq. (C9), note that, since $R(qT)\mathbf{a} = \mathbf{a}$, $\partial_x(R\mathbf{a}) = \partial_x\mathbf{a}$. Using the chain rule, we also have $\partial_x(R\mathbf{a}) = (\partial_x R)\mathbf{a} + R\partial_x\mathbf{a}$. Equating the two expressions, we obtain

$$(\partial_x R)\mathbf{a} = (1 - R)\partial_x\mathbf{a}. \tag{C10}$$

From the spectral decomposition of R, we have, for any vector $\mathbf{v}$, $|(1 - R)\mathbf{v}| \geq |e^{-i\delta\varepsilon T} - 1||\mathbf{v}|$. Using this result along with $|e^{-i\alpha} - 1| \geq \alpha\pi/2$ in the equation above, we obtain $|\partial_x R\mathbf{a}| \leq \delta\varepsilon qT\pi|\partial_x\mathbf{a}|/2$. Using $|\partial_x R\mathbf{a}| \leq \|\partial_x R\|$, Eq. (C9) follows.

Using the chain rule and the triangle inequality, one can verify $\|\partial_x R(x, p, qT)\| \leq \int_0^{qT} dt\|\partial_x H^{(3)}(x, p, t)\|$. Since $\|\partial_x H_q(x, p, t)\| \leq \eta|\partial_x\mathbf{h}| = \eta$, we then find $\|\partial_x R(x, p, qT)\| \leq \eta qT$. Thus, we conclude

$$|\partial_x\mathbf{a}| \leq \frac{2\eta}{\pi\delta\varepsilon(x, p)}. \tag{C11}$$

The same bound holds for $|\partial_p\mathbf{a}|$ by similar arguments. Using Eq. (C11) along with $\dot{x}, \dot{p} \leq \eta + \delta\omega A$ [see Eqs. (9)-(10)] and the triangle inequality, we obtain

$$\left|\frac{d}{dt}\mathbf{a}\right| \leq \frac{4\eta}{\pi\delta\varepsilon(x, p)}(\eta + A\delta\omega). \tag{C12}$$

Hence, using $4/\pi \sim 1$, the condition $|d\mathbf{a}/dt| \ll \delta\varepsilon$ is satisfied when

$$\delta\varepsilon^2 \gg \eta^2,\, \eta\delta\omega A. \tag{C13}$$

These are the first two conditions quoted in Eq. (21).

The latter two conditions in Eq. (21) come from requiring that $\tilde{x}$ and $\tilde{p}$ remain stationary within a driving period. This condition allows integrating out the time-dependence, similar to Sec. II B in the main text. The quasistationarity condition is $\Delta x(t), \Delta p(t) \ll A$ for $t < qT$. From the same line of arguments as in Sec. II B (using $|\dot{x}|, |\dot{p}| \leq \delta\omega A + \eta$), we find that this condition is satisfied when $\delta\omega qT \ll 1$ and $\eta qT \ll A$. These are the two last conditions quoted in Eq. (21).

b. Derivation of effective Hamiltonian

We now derive the effective Hamiltonian in Eq. (19). In the Floquet regime, whose conditions were identified above, the discussion in Sec. II B 2 implies that

$\mathbf{S}(t) = \pm \mathbf{n}_0(x, p, t)$ in Eqs. (9)-(10), when the spin is initially aligned or anti-aligned with the stroboscopic precession axis: $\mathbf{S}(0) = \pm \mathbf{a}(x(0), p(0))$. Using this in Eqs. (9) and (10), we obtain

$$\dot{x} = v_x(x, p, t), \quad \dot{p} = -v_p(x, p, t), \qquad \text{(C14)}$$

where, for $s = x, p$,

$$v_x(x, p, t) \equiv \delta\omega p \pm \eta \partial_p \mathbf{h}(t) \cdot \mathbf{n}_0(x, p, t), \quad \text{(C15)}$$
$$v_p(x, p, t) \equiv \delta\omega x \pm \eta \partial_x \mathbf{h}(t) \cdot \mathbf{n}_0(x, p, t). \quad \text{(C16)}$$

Since the state of the cavity is effectively stationary on the timescale of the driving field qT, we may integrate out the time-dependence of $v_x(x, p, t)$, obtaining

$$\dot{x} \approx \bar{v}_x(x, p), \quad \dot{p} \approx \bar{v}_p(x, p), \qquad \text{(C17)}$$

where, for $s = x, p$,

$$\bar{v}_s(x, p) = \delta\omega s \pm \frac{\eta}{qT} \int_0^{qT} dt\, \partial_s \mathbf{h}(x, p, t) \cdot \mathbf{n}_0(x, p, t). \quad \text{(C18)}$$

The goal of this subsection is to show that $\bar{v}_x = \partial_p H_{\mathrm{eff}}(x, p)$ and $\bar{v}_p = \partial_x H_{\mathrm{eff}}(x, p)$, where $H_{\mathrm{eff}}(x, p)$ is given in Eq. (19). To do this, we first use the chain rule to rewrite the integrand in the second term above for $s = p$ (the case $s = x$ follows analogously)

$$\partial_p \mathbf{h} \cdot \mathbf{n}_0 = \partial_p [\mathbf{h} \cdot \mathbf{n}_0] - \mathbf{h} \cdot \partial_p \mathbf{n}_0, \qquad \text{(C19)}$$

where we suppressed the above quantities' dependence on x, p, and t for brevity. We now consider the last term above. Since $\mathbf{n}_0$ obeys the Bloch equation [Eq. (11)] $\partial_t \mathbf{n}_0 = -\eta \mathbf{h} \times \mathbf{n}_0$, we may write

$$\mathbf{h} = \mathbf{n}_0 (\mathbf{h} \cdot \mathbf{n}_0) - \frac{1}{\eta} \mathbf{n}_0 \times \partial_t \mathbf{n}_0. \qquad \text{(C20)}$$

This result can be proven by directly inserting $\partial_t \mathbf{n}_0 = -\eta \mathbf{h} \times \mathbf{n}_0$ into the above, and using the cross product identity $\mathbf{a} \times (\mathbf{b} \times \mathbf{c}) = \mathbf{b}(\mathbf{a} \cdot \mathbf{c}) - \mathbf{c}(\mathbf{a} \cdot \mathbf{b})$ along with $\mathbf{n}_0 \cdot \mathbf{n}_0 = 1$. Using the above result along with $\mathbf{n}_0 \cdot \partial_p \mathbf{n}_0 = 0$ (recall that $\mathbf{n}_0$ is normalized), we obtain

$$\mathbf{h} \cdot \partial_p \mathbf{n}_0 = -\frac{1}{\eta} (\mathbf{n}_0 \times \partial_t \mathbf{n}_0) \cdot \partial_p \mathbf{n}_0. \qquad \text{(C21)}$$

Using $(\mathbf{a} \times \mathbf{b}) \cdot \mathbf{c} = \mathbf{b} \cdot (\mathbf{c} \times \mathbf{a})$, and substituting into Eq. (C19), we find

$$\partial_p \mathbf{h} \cdot \mathbf{n}_0 = \partial_p [\mathbf{h} \cdot \mathbf{n}_0] + \mathbf{n}_0 \cdot (\partial_t \mathbf{n}_0 \times \partial_p \mathbf{n}_0).$$

We identify the second term as the the x-Berry flux $F_x(x, p, t)$ associated with the mapping of $\mathbb{R}^3$ to the

unit sphere defined by $\mathbf{n}_0(x, p, t)$. One can verify that $\int_0^{qT} dt\, F_x(x, p, t) = \partial_p \gamma(x, p)$, where $\gamma(x, p)$ denotes the Berry phase associated with the loop traversed by $\mathbf{n}_0(x, p, t)$ on the unit sphere for $0 \le t < T$. Thus,

$$\frac{\eta}{qT} \int_0^{qT} dt\, \partial_p \mathbf{h} \cdot \mathbf{n}_0 = \frac{\partial}{\partial p} \left(\frac{\eta}{qT} \int_0^{qT} dt\, \mathbf{h} \cdot \mathbf{n}_0 + \frac{1}{qT} \gamma \right).$$

Using this in Eq. (C18), we obtain

$$\bar{v}_x(x, p) = \frac{\partial}{\partial p} \left(\frac{\delta\omega}{2}(x^2 + p^2) + \frac{1}{qT} \gamma(x, p) \right.$$
$$\left. \pm \frac{\eta}{qT} \int_0^{qT} dt\, \mathbf{h}(x, p, t) \cdot \mathbf{n}_0(x, p, t) \right),$$

where we restored the dependence on x and p.

The final step is to show that the term inside the parentheses above equals the quasienergy $\varepsilon(x, p)$ of the Hamiltonian $H^{(3)}(x, p, t)$. To show this, we recall that the Bloch equation $\partial_t \mathbf{S}(t) = -\eta \mathbf{h}(t) \times \mathbf{S}(t)$ describes the evolution of the expectation value of $\hat{\mathbf{S}}$ with the qT-periodic spin-1/2 Hamiltonian $\hat{H}_s(t) = \eta \mathbf{h}(t) \cdot \hat{\mathbf{S}}$ (here we suppressed the dependence of $\mathbf{h}$ and $\hat{H}_s$ on x and p). Noting that the stroboscopic time-evolution of $\langle \mathbf{S} \rangle$ is generated by a rotation by the angle $\varepsilon_0 T$ around the axis $\mathbf{n}_0$ [see Eq. (C8)], we conclude that the Floquet operator generated by $\hat{H}_s(t)$ is a 2×2 unitary matrix given by $\hat{U}_s(qT) = e^{-i\varepsilon T \mathbf{n}_0(0) \cdot \hat{\mathbf{S}}}$. Thus, we identify ε as the (positive) quasienergy associated with $\hat{H}_s(t)$.

To obtain an expression for ε, we note that $|\psi(t)\rangle = e^{-i\varepsilon t}|\phi_+(t)\rangle$ solves the Schrödinger equation generated by $\hat{H}_s(t)$, where $|\phi_+(t)\rangle$ denotes the Floquet state of $\hat{H}_s(t)$ with quasienergy ε. Thus, by direct substitution, one can verify that

$$\varepsilon = \frac{i}{qT} \int_0^{qT} dt\, \langle \psi(t)|\partial_t|\psi(t)\rangle - \frac{i}{T} \int_0^{qT} dt\, \langle \phi_+(t)|\partial_t|\phi_+(t)\rangle. \qquad \text{(C22)}$$

We have $\langle \psi(t)|\partial_t|\psi(t)\rangle = i\eta \mathbf{n}(t) \cdot \mathbf{h}(t)$, where $\mathbf{n}(t)$ denotes the Bloch vector of the state $|\psi(t)\rangle$, which obeys the Bloch equation [Eq. (11)], and is identical to the Bloch vector of $|\phi_+(t)\rangle$. Since $|\phi_+(t)\rangle$ is time-periodic, $\mathbf{n}(t)$ is a time-periodic solution to the Bloch equation Eq. (11), and we thus identify $\mathbf{n}(t) = \mathbf{n}_0(t)$ (the sign follows from the initial conditions). Identifying the latter term above as the Berry phase $\gamma(x, p)$ (with a factor of $1/qT$), and restoring x and p, we conclude

$$\varepsilon(x, p) = \frac{\eta}{qT} \int_0^{qT} dt\, \mathbf{h}(x, p, t) \cdot \mathbf{n}_0(x, p, t) + \frac{1}{qT} \gamma(x, p). \qquad \text{(C23)}$$

A similar result holds for $\bar{v}_p$. This was what we wanted to show, and concludes this Appendix.